Modelling Room Temperature Ionic Liquids: Charge Environment, Hydrogen Bond Dynamics and Related Phenomena

A Thesis

Submitted For the Degree of

MASTER OF SCIENCE (ENGINEERING)

in the Faculty of Science

by

Avula Venkata Siva Nikhil

CHEMISTRY AND PHYSICS OF MATERIALS UNIT
JAWAHARLAL NEHRU CENTRE FOR ADVANCED SCIENTIFIC RESEARCH
Bangalore – 560 064, India

JANUARY 2019

To My Family

DECLARATION

I hereby declare that the matter embodied in the thesis entitled "**Modelling Room Temperature Ionic Liquids: Charge Environment, Hydrogen Bond Dynamics and Related Phenomena**" is the result of investigations carried out by me at the Chemistry and Physics of Materials Unit, Jawaharlal Nehru Centre for Advanced Scientific Research, Bangalore, India under the supervision of Prof. S. Balasubramanian and that it has not been submitted elsewhere for the award of any degree or diploma.

In keeping with the general practice in reporting scientific observations, due acknowledgement has been made whenever the work described is based on the findings of other investigators. Any omission that might have occurred by oversight or error of judgement is regretted.

Avula Venkata Siva Nikhil

CERTIFICATE

I hereby certify that the matter embodied in this thesis entitled "**Modelling Room Temperature Ionic Liquids: Charge Environment, Hydrogen Bond Dynamics and Related Phenomena**" has been carried out by Mr. Avula Venkata Siva Nikhil at the Chemistry and Physics of Materials Unit, Jawaharlal Nehru Centre for Advanced Scientific Research, Bangalore, India under my supervision and that it has not been submitted elsewhere for the award of any degree or diploma.

Prof. S. Balasubramanian
(Research Supervisor)

Acknowledgements

The two years of my master's study at JNCASR has been a transformational experience for me both professionally and personally. I have learnt a lot about life and research from the people that I met here and I am grateful to them.

It gives me great pleasure to thank my research supervisor Prof. S. Balasubramanian for introducing me to the field of scientific research. He has given me the freedom to explore the field of computational chemistry but has never shied away from correcting me when I was drifting too far. It is only because of him that I got a thorough exposure to research methodologies. I will always be indebted to him.

I thank JNCASR for providing state of the art research facilities. I would like to thank the faculty of CPMU, TSU and EMU for the courses they offered.

I am thankful to TUE-CMS for providing the computational resources for carrying out my research. I thank JNCASR, DST for funding. I thank all the academic and non-academic staff of JNCASR for their support. I acknowledge the open source community for their efforts in building the software that I used for my research.

I thank all my present and past lab-mates - Satya, Karteek, Anirban, Tarak, Sudip, Divya, Sourav, Saibal, Nimish, Srinath, Sudarshan, Anjali, Srimayee and Rahul - for their help and support. I have learnt a lot from them and certainly made my stay at JNCASR a pleasant one. I thank all my friends and batchmates for the moments that I shared with them.

Finally, I thank my parents, sister and family for their unconditional support in all my pursuits.

Preface

The thesis encompasses studies on modelling of room temperature ionic liquids using molecular simulations. In particular, insights from the investigation of the charge environment in imidazolium-based binary ionic liquid mixtures are reported. A multiscale approach - combining inputs from Density Functional Theory (DFT) and classical Molecular Dynamics (MD) simulations - developed for this study is described. The estimation of hydrogen bond exchange timescales to resolve apparently conflicting experimental observations is described. Preliminary findings on the validation of MD force field for oligomeric ionic liquids are presented. Relations to experimental findings and data are reported, wherever possible.

Chapter 1 presents a general introduction to the methods and tools used for the investigations described below. A brief summary of the relevant physicochemical properties of ionic liquids is provided. A review of previous work, representative though non-exhaustive, on modelling of ionic liquids is also presented.

Chapter 2 is divided into two subchapters. **Chapter 2A** describes the investigation of the charge environment in an imidazolium-based binary ionic liquid mixture, [BMIM][Cl][BF_4]. The fidelity of an MD force field to quantitatively describe the dynamic properties of ionic liquids is contingent upon the use of accurate condensed phase atomic site charges. A consistent framework to obtain and integrate atomic site charges into a force field was developed earlier. This thesis extends this framework to binary mixtures of ionic liquids. In sum, classical MD simulations at room temperature are employed to sample the liquid configurations for a subsequent geometry optimization in DFT framework.

Subsequently, the Density Derived Electrostatic and Chemical (DDEC) charge partitioning method is used to derive atomic site charges from electron densities. This procedure is applied to seven compositions of [BMIM][Cl][BF_4] system. Analysis of the net ion charges (NICs) showed that the cation's (BMIM) charge varies linearly with anion composition, whereas the anion charges remain invariant. An X-ray Photoelectron Spectroscopy (XPS) study of a similar ionic liquid mixture by Licence *et al.* revealed that the N 1s binding energy of the cation varies linearly with composition, whereas that of anion remains invariant. This experimental result serves as direct evidence to our findings.

Chapter 2B describes the hydrogen bond exchange process in the same binary mixture. Doseok *et al*. used IR and NMR experiments to study the hydrogen bond environment in [BMIM][Cl][BF_4]. A discrepancy was observed, with IR spectra indicating two distinct hydrogen bond environments and NMR showing only one. A difference in the time scales of IR and NMR techniques was thought of as the probable cause for this discrepancy. We estimated the time scales of exchange of hydrogen bonds between the cation and the two anions. We defined a time-dependent pair correlation function to describe this phenomenon quantitatively. The timescales of exchange were shown to be in nanoseconds which is in between the timescale of IR method (picosecond) and NMR method (microsecond), hence resolving the discrepancy.

Chapter 3 describes the validation of a force field for a new class of ionic liquids called oligomeric ionic liquids (OILs). Aida *et al.* reported that, by linking imidazolium cations via an ether linkage, double layer capacitance of devices using ILs could be improved six-fold. To accurately model this class of ionic liquids, a general force field needs to be systematically refined. We used the General Amber Force Field (GAFF) force field, along with some modified parameters for ether linkage, to study this system. A representative set of gas phase conformers was created by geometry optimization in DFT framework. Atomic site charges were then refined using a iterative procedure by simultaneously fitting the electrostatic potential of multiple configurations using the Restrained ElectroStatic Potential (RESP) procedure. These charges were then used to simulate the bulk liquid and

the IL-vacuum interface. Due to the sluggish behaviour of OILs, multiple independent trajectories generated by a charge scaling procedure were used to analyze the results. Density and surface tension values from simulations are found to be in good agreement with experimental values. Preliminary findings of local and interfacial structure reveal striking similarities with that of monomeric ionic liquids.

Chapter 4 summarizes the thesis and provides a brief future outlook. Interfacial structure of binary ionic liquids could be studied to investigate selective enrichment near the surface. Mesoscopic structure could be studied to examine any structural differences between monomeric and oligomeric ionic liquids.

Contents

List of Figures

List of Tables

Chapter 1

Introduction

In simple terms, room temperature ionic liquids (RTILs) are materials that are composed entirely of ions (without any charge neutral molecules) and also melt at low temperatures. [1–8] While 100^oC is generally accepted as an arbitrary upper limit on melting point of RTILs, there is no fundamental difference between salts that melt at say 80^oC and those at 120^oC. [3] Low melting nature of RTILs does present a clear advantage over high temperature molten salts in terms of ease of handling without the need of special equipment. [3]

Paul Walden is credited to have synthesized in 1914 the earliest RTIL $[EtNH_3][NO_3]$ which had a melting point of 12^oC. [3, 9] There were many other independent scattered discoveries of other RTILs until early 1980s. These early RTILs were mainly based on chloroaluminate salts and had severe limitations with regards to their stability when exposed to air or moisture. It was in the early 1990s that air and moisture stable RTILs were developed and these diverse compounds started to be viewed under the single lens of RTILs. [3, 9]

Ionic liquids (ILs) have many unique properties such as low vapor pressure, large liquid range, high thermal stability, wide electrochemical window etc. which allow them to be utilized in a diverse range of applications like separation processes, gas capture, catalysis, bio-catalysis, energy storage, energy generation, lubrication etc. [10–40] Though there are a couple of instances of RTILs being used in industry scale commercial applications (like

BASF's BASIL^{TM} process), there are many more potential areas of applications that have not yet been realized. [41]

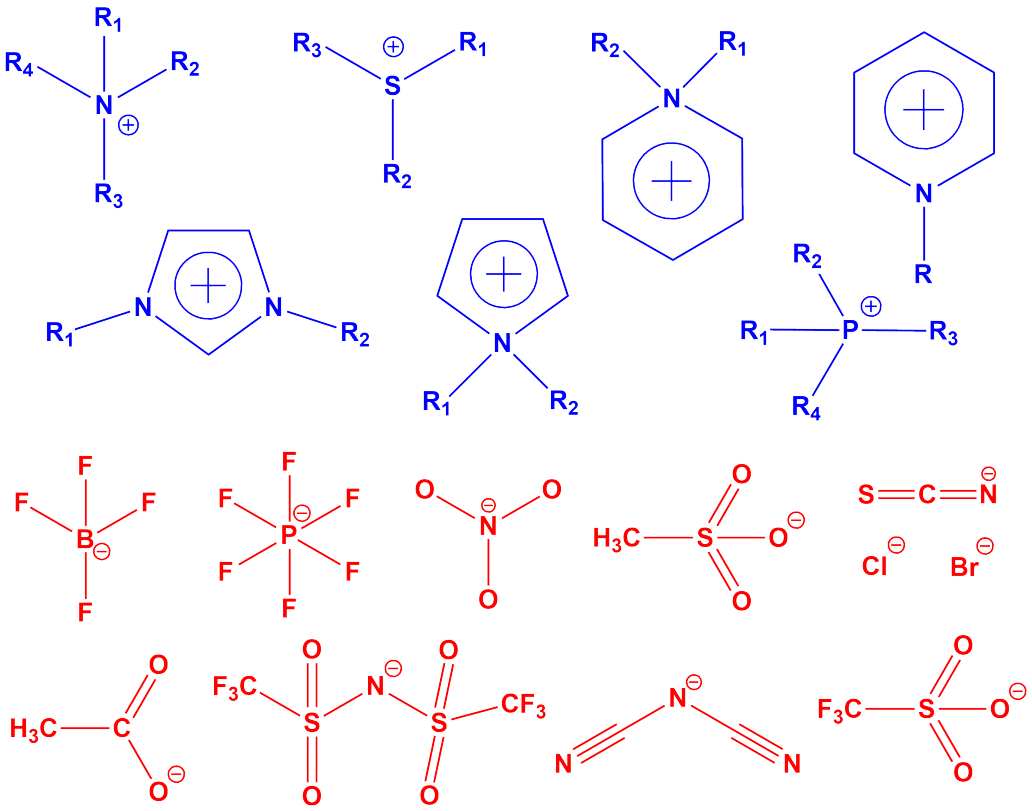

Figure 1.1: Schematic picture of a representative set of ions used in RTILs.

1.0.1 Interactions in a prototypical ionic liquid

Figure 1.1 shows some of the commonly used ions in ILs. In principle, one can tune the properties of a solvent by choosing the right combination of ions for a given application. This kind of combinatorics can result in more than a million possible ILs, and are hence touted as "designer solvents". [5] Ionic liquids with imidazolium cations are the most commonly used and studied. [3]

Imidazolium based cations have a ring part and a tail part as shown in Figure 1.2. ILs exhibit an array of competing interactions. There is a strong attractive electrostatic interaction between oppositely charged ions, hydrogen bonding interaction between ring hydrogens and anions, dispersion interactions between the alkyl tails and $\pi - \pi$ stacking interactions between the cation rings. [4, 42] The relative dominance of one interaction over

the other changes from system to system. For example, imidazolium based ILs with alkyl side chains longer than butyl tend to aggregate into non-polar domains. These non-polar domains become more connected as the length of the alkyl side chain increases and with C12 side chain, a continuous network of non-polar domains separated by small pockets of polar domains are observed. [3, 7, 43, 44] The strength of the hydrogen bond also depends on the combination of cation and anion chosen, with more basic anions forming stronger hydrogen bonds than the less basic ones. [45] The varying strength of hydrogen bond has many consequences, primary ones being the local solvation shell structure and charge transfer between the ions (see chapter 2A for further discussion). [45, 46] In essence, there is always an interplay of interactions in ILs with electrostatic interaction being the ubiquitous one and which interaction dominates depends on the choice of cation-anion combination.

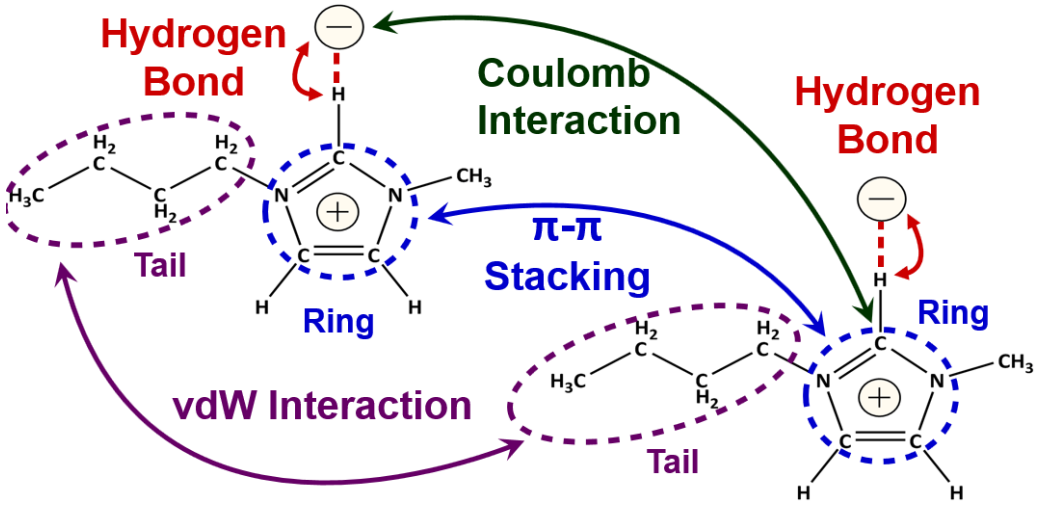

Figure 1.2: Schematic of imidazolium based IL and the various interactions involved.

1.0.2 Applications of ILs

As mentioned earlier, ILs are now being investigated for a wide variety of applications from nuclear to space industry. [19, 47] Some of the common applications of the ILs are presented here.

Solvent

ILs from their inception have been investigated as solvents. [1–3, 48] Ability to tune the properties and the negligible vapor pressure make ILs a suitable candidate to replace volatile organic solvents (VOCs). [49] These properties are also the reason that ILs are considered widely as "green solvents". One of the major applications of ILs as solvents is biomass dissolution. [5, 50–52] Biomass is an abundant, underutilized and promising alternative to traditional non-renewable energy sources, but conversion of biomass to biofuel is rather challenging. [22] Biomass is difficult to dissolve in water, traditional organic solvents and requires harsh conditions to process. [5, 7, 50] ILs were shown to dissolve cellulose under mild conditions without any pretreatment. [22, 50] Though there are many challenges yet to be overcome, this field still remains an area of intense study. [22]

Electrolyte

ILs have good conductivity, wide electrochemical window and are non-flammable. These properties make ILs contenders to replace flammable and volatile organic solvent electrolytes that are currently being used. [20, 53–58] Protic ionic liquids (PILs) can conduct protons without being hydrated and are hence being investigated for their use in proton-exchange membrane (PEM) fuel cells. [59–61] Recently ILs are being used as gate materials in single molecule transistors. [62] Wide liquid range, wide electrochemical window and large electric doubl layer (EDL) capacitance of ILs give them a clear edge over traditional aqueous electrolytes. [63, 64] Ionic liquids are also being investigated as potential electrolytes for supercapacitors and a recent class of ionic liquids called oligomeric ionic liquids (OILs) holds much promise in this field. [64–68]

Gas dissolution

Brennecke *et al.* have demonstrated the use of mixtures of ILs and CO_2 for separation of various organic compounds which led to a huge amount of work into understanding the IL-CO_2 mixtures. [69–71] CO_2 has excellent solubility in many ILs, and moreover, as ILs are excellent solvents for catalysis, they can be used to capture and convert CO_2 to other

products. [18, 71–73] Anions were found to influence the CO_2 solubility to a larger extent than cations, with CO_2 molecules filling the voids surrounding the anions. [74] Recently, amino acid ionic liquids (AAILs) were used to dissolve much higher (10% mass capacity) quantities of CO_2 by using chemisorption instead of physical dissolution. [75]

1.0.3 Simulation methods

There are many excellent books and articles describing in detail the simulation methods used in this thesis. [76–86] A brief description of the theoretical tools underlying the simulations is provided in this section. Most of these tools are well established, and hence, rather than presenting systematic derivations some crucial aspects related to their applications are described.

Classical molecular dynamics

Classical molecular dynamics (MD) simulations as the name suggests is a mathematical framework that solves for the time evolution of particles (in this case atoms/molecules), given the interactions (called force field) between them are known in advance. MD simulations obtain the time evolution of the system by solving Newton's equations of motion using discrete time step integrators. [76–79] Using a typical MD simulation one can investigate systems of nanometer length scale for a duration of the order of 100s of nanoseconds. Periodic boundary conditions (PBCs) are generally applied to the simulation box to simulate bulk like environment. SSystems can be simulated at constant pressure, temperature and potential with the equations of motion modified by coupling with appropriate barostats, thermostats etc. [87–89] It is also possible to simulate systems under external perturbations (non-equilibrium molecular dynamics) like shear, electric field etc making MD especially useful in the areas such as molecular rheology and nanofluidics. [90]

The fidelity of an MD simulation depends on the choice of force field used. [91, 92] Most MD simulations use effective pair potentials to describe the many-body interactions between the particles. In the context of ionic liquids simulations, force fields should be able to capture both the strong and weak interactions that are at play in the condensed phase. The

Coulomb interaction between the ions is captured by assigning point charges to each atom of the ions. The dispersion interactions are captured by the Lennard-Jones (LJ) potential. The conformational flexibility of the ions is captured by the intramolecular bonded potential terms (like bond, angle and dihedral terms). Presence of hydrogen bonding between the cation and anion leads to significant charge transfer, hence the charge and LJ parameters are interlinked. [93, 94] A careful parametrization scheme is needed to capture the multitude of interactions present in ionic liquids.

The advantage of MD simulations over other techniques like Monte Carlo (MC) simulations and classical density functional theory (CDFT) is the ability to describe local structure (like solvation shell structure), bulk structure (structure factor) and dynamical processes (diffusion, hydrogen bond dynamics etc.) simultaneously. The average properties of the system under study are calculated as the time averages of various functions. In principle MD simulations are time origin independent, hence a further averaging over the choice of time origin can improve the predicted results. Some of the experimental quantities that can be estimated using MD are density, structure factor, diffusion constant, surface tension, enthalpy of vaporization, viscosity, conductivity etc.

Though MD offers a gamut of applications, it has severe limitations on the length and time scales that are accessible by the simulations. The length scale problem can be overcome by using coarse-grained force fields, implicit solvent methods, patchy particle models etc. [95–97] But accessing higher time scales still remains a bottle neck. [98]

Quantum chemical calculations

As opposed to MD, quantum chemical calculations take into account electronic degrees of freedom explicitly. This allows for phenomena like charge transfer and polarization to be studied in detail. Density functional theory (DFT) based methods are used to estimate the electron density in this thesis. In density functional theory, the energy of the system is expressed as the functional of the electron density. [84, 85] As opposed to other quantum chemical calculations (like post-Hartree-Fock (HF) methods) which solves for electron wave functions, DFT solves for the electron density of the system. DFT scales as N^3

with the number of electrons (there is lot of ongoing research on linear scaling DFT) whereas, post-HF methods scale as N^4 making DFT the preferred option for relatively large system sizes. [85] The condensed phase systems of ionic liquids investigated in chapter 1.0.6 typically contain ≈2000 electrons which is beyond the capabilities of the post-HF methods. [85] Many studies have demonstrated that DFT does not accurately capture the dispersion interactions. Explicit inclusion of Grimme's dispersion corrections solves this issue to some extent. [99]

Geometry optimization using DFT moves the coordinates of the nuclei to minimize the force on them. Traditional geometry optimization using DFT generally converge to local minimum in energies rather than exploring the entire configurational space to find the global minimum of energy. Therefore, in the context of viscous ionic liquids, it is important to start geometry optimizations from several configurations. In order to explore configurations inaccessible to human intuition configurations selected from a MD simulation can be used as starting configurations. In chapter 2B.4, such sampling from MD runs has resulted in a more representative and trustworthy configurations.

Atomic site charges

Classical molecular dynamics simulations do not solve for the electronic degrees of freedom and hence, can capture only a mean field picture of the electron distribution via atomic site charges. Condensing the information contained in the electron density description into atomic site charges results in an obvious loss of information (higher multipoles are ignored). Hence, there is no unique method to determine these atomic site charges and there exists many ways to determine them. Some of the popular methods for atomic population analysis are listed here –

- Mulliken population analysis
- Bader's quantum chemical topology (QCT) [100]
- Electrostatic potential fitting methods (ESP, RESP, Chelpg, REPEAT) [101]
- The Hirshfeld method [102, 103]

- Natural population analysis (NPA) [104]
- Density derived electrostatic and chemical (DDEC) charges [105–110]

Mulliken charges are heavily dependent on the choice of basis set used to describe electrons, hence difficult to choose unique values independent of the basis sets. [104] Bader's QCT can lead to non-nuclear attractors resulting in point charges located away from nuclei which are difficult to implement in MD. [100] ESP charges are fitted to reproduce the electrostatic potential of the quantum electron density and are meaningful to incorporate in MD framework. But ESP charges suffer from buried atoms (atoms whose distance from the van der Waals surface is smaller than their van der Waals radii) getting inaccurate charges. [101] Hirshfeld method is based on neutral atom reference electron densities and hence underestimates the atomic charges. [102, 103]

In order to overcome such defects, Manz and Sholl proposed a density derived electrostatic and chemical (DDEC) method. In this scheme the electron density is partitioned into single atom electron density distributions. [105–110] They construct the method based on the following performance goals [108] –

- Only one electron distribution should be assigned to each atom.
- Core electrons should contribute only to the parent atom.
- Atomic site charges should be functionals of the total electron density distribution.
- Atomic site charges should be consistent with electronegativity trends.
- Atomic site charges should be transferable across different conformations of the molecule.
- Convergence to the final solution should be robust and stable.
- Computational cost should scale linearly with the number of electrons.

DDEC charges were tested on a range of different materials – porous solids, ionic solids, small and large molecules, organometallics, nanoclusters, solid surfaces. [108] Sholl *et al.*

applied DDEC method to generate a large publicly available database of atomic site charges for over 3000 metal organic framework (MOF) structures. [111] The broad applicability of DDEC method to various materials makes it a strong contender to be considered as a default method to estimate atomic site charges. Mondal and Balasubramanian found that DDEC method yielded consistent charges for imidazolium based ionic liquids when compared to RESP, REPEAT and Blöchl methods. [94, 112]

1.0.4 Review of recent work

There are many review articles which chronicle the efforts of the scientific community to model ionic liquids. [113–115] This section presents some of the recent relevant work on modelling of ionic liquids.

Lopes and Pádua developed a general force field based (CL&P) on OPLS-AA model for ionic liquids including a wide class of anions and cations. [116–120] The force field is based on three basic tenets – (i) internal consistency, (ii) transferability and (iii) compatibility. Cations and anions in an ionic liquid have distinct chemical properties and generally belong to different classes of molecules. For instance many of the cations are organic molecules for which force field parameters are available with general force fields like AMBER, GAFF, OPLS etc. But the same general force fields might not have parameters for anions which are mostly inorganic (GAFF has all the force field parameters for imidazolium cations but lacks parameters for common anions like [PF_6]). In the absence of a consistent force field for ionic liquids, it was common to see parametrizations of cations and anions adopted from different general force fields which might not always be compatible (GAFF and OPLS have different 1-4 scaling parameters). [121–123] The first tenet of the CL&P force field solves this issue by using the functional rules of OPLS-AA force field for all cations and anions uniformly. [122, 123] Though specific parametrization can improve the accuracy of the force field, it comes at the cost of transferability. For example same parameters should be applied to a homologous family of molecules (like cations with different side chain lengths). The second tenet imposes restrictions on parametrization to account for the transferability of the force field. Finally, parametrizations of ionic liquids should be compatible with other

common neutral molecules (H_2O, CO_2 etc.) to enable studies involving mixtures of ionic liquids and other molecules. CL&P force field is based on OPLS-AA force field thereby making it compatible with a wide variety of neutral molecules. CL&P force field could predict accurately many structural and thermodynamic properties of ionic liquids. Using this force field, Lopes and Pádua predicted that imidazolium cation based ionic liquids show nanostructuring for cations of tail length greater than C4, which was later confirmed by experiments. [43, 124] This was one of the rare happy instances of simulations preceding experimental observations.

In spite of all the merits of CL&P force field, it has severe drawbacks in capturing dynamic properties and hydrogen bonding in ionic liquids. [46, 94, 112] One of the main reasons for this failure is its inability to capture charge transfer between cation and anion. Quantum chemical calculations of ion pairs in gas phase show that there is significant amount of charge transfer between cation and anion resulting in the reduction of the magnitude of the net charges of the ions. Holm *et al.* systematically compared structural and dynamic aspects of two commonly used full charge models (force fields with net charge of ions to be $\pm$ 1). They conclude that though structural properties are captured well, the dynamic properties (like diffusion constant) are well below the experimental values. [46] They attribute this failure to derivations of the atomic site charges from the gas phase quantum chemical calculation of single ion (as opposed to ion pairs or bigger clusters). Holm *et al.* compared the charges obtained from gas phase MP2 calculations and Car-Parrinello molecular dynamics (CPMD) run of 30 ion pairs of [DMIM][Cl] system using Blöchl method. [93] Both calculations show that there is a significant reduction in the net charge of the ions from ± 1 to ± 0.63. Results from CPMD run also show that there are large fluctuations in atomic site charges indicating that the polarization also plays an important role. In another work, Holm *et al.* found that the atomic site charges derived from quantum chemical calculations of ion clusters depended on the local structure of the ions. [125] Hence, they suggest that the atomic site charges should be calculated from liquid state configurations rather than single ions or ion pairs. They also found that the

electric dipole distribution on the ions is independent of the temperature of the liquid phase simulations. [125] Holm *et al.* also proposed a refined force field for imidazolium based ionic liquids using *ab-initio* charges, which showed better agreement of dynamic properties like conductivity with experimental values when compared to CL&P force field. [126]

Maginn *et al.* studied [BMIM][PF_6] system using GAFF force field with a set of charges obtained from a different protocol. [127] They estimated the atomic site charges from crystal DFT and liquid state AIMD simulations. When compared with simple scaled charges (charges obtained from single ion and scaled by factor of 0.8) *ab-initio* charges showed better properties. Hence, they conclude that apart from the net charge of the ion, the atomic site charge distribution in the ion is also important. Mondal and Balasubramanian systematically refined the CL&P force field starting from *ab-initio* charges derived from crystal or condensed phase periodic DFT calculations. [94, 112] Work presented in Chapter 2 of this thesis is based on this method of estimating atomic site charges from condensed phase periodic DFT calculations.

Hunt *et al.* studied the lifetime of hydrogen bonds between the cation and the anion in [EMIM][Cl] and [BMIM][Cl] systems using classical MD simulations. [128] They studied the dependence of lifetimes on the geometric criteria (angle and bond distance cutoff) used to define a hydrogen bond. They conclude that the breaking of hydrogen bonds is primarily due to the angular motion of the anion around a cation than the translational motion of anion away from the cation. They also estimated the lifetimes of hydrogen bonds of the anion with different hydrogens on the cation (ring, methylene and tail). They found that ring hydrogens form the strongest (in terms of the hydrogen bond lifetime) hydrogen bonds followed by methylene and tail hydrogens, which is to be expected from the static structure (with anions clustering near ring hydrogens). Kirchner *et al.* studied hydrogen bonding dynamics in [EMIM][SCN] using AIMD and found an unexpected result that the H_A (Figure 2A.2) hydrogen bond decays faster than H_B hydrogen bond. [129]

Recently Wu *et al.* investigated a new class of ionic liquids called oligomeric ionic liquids (OILs) using classical density functional theory (CDFT). [130] They conclude

that oligomeric cations have little improvement to the charging behavior on the positive electrode while they enhance the energy storage density at the negative electrode. This is to be expected as the structure of electric double layer (EDL) at the positive electrode would be rich in anions and that of negative electrode would be rich in cations. Though CDFT calculations give some insight into the capacitive behaviour of OILs at interfaces, this model is too coarse grained to consider the details of the linkers. Aida *et al.* noted that the choice of linkers can have drastic effects on the properties (like viscosity) of the system. [65]

1.0.5 Software used

All molecular dynamics (MD) simulations were performed using LAMMPS software. [131–133] GaussView and Gaussian 09 software were used to construct gas phase configurations of molecules and run gas phase quantum geometry optimizations. [134, 135] Packmol was used to pack ion pairs into an MD simulation box for the starting configuration of liquid simulations. [136] Periodic DFT based geometry optimizations were performed using CP2K software. [137] Chargemol program was used to calculate the atomic site charges from electron densities using the DDEC/c3 scheme. [105, 106] Ambertools, Red-tools and intermol packages were used to obtain GAFF force field parameters for oligomeric ionic liquid (OIL) system. [101, 121, 138, 139] Visualization of the trajectories was done using VMD along with topotools plugin. [140] Finally, analysis codes were written in FORTRAN with OPENMP parallelization and wrapped with bash scripts wherever necessary.

1.0.6 Scope of the thesis

The thesis encompasses studies on modelling of room temperature ionic liquids using molecular simulations. In particular, insights from the investigation of the charge environment in imidazolium-based binary ionic liquid mixtures are reported. A multiscale approach - combining inputs from Density Functional Theory (DFT) and classical Molecular Dynamics (MD) simulations - developed for this study is described. The estimation of hydrogen bond exchange timescales to resolve apparently conflicting experimental observations is

described. Preliminary findings on the validation of MD force field for oligomeric ionic liquids are presented. Relations to experimental findings and data are reported, wherever possible.

Chapter 1 presents a general introduction to the methods and tools used for the investigations described below. A brief summary of the relevant physicochemical properties of ionic liquids is provided. A review of previous work, representative though non-exhaustive, on modelling of ionic liquids is also presented.

Chapter 2 is divided into two subchapters. **Chapter 2A** describes the investigation of the charge environment in an imidazolium-based binary ionic liquid mixture, [BMIM][Cl][BF_4]. The fidelity of an MD force field to quantitatively describe the dynamic properties of ionic liquids is contingent upon the use of accurate condensed phase atomic site charges. A consistent framework to obtain and integrate atomic site charges into a force field was developed earlier. [94, 112] This thesis extends this framework to binary mixtures of ionic liquids. In sum, classical MD simulations at room temperature are employed to sample the liquid configurations for a subsequent geometry optimization in DFT framework. Subsequently, the Density Derived Electrostatic and Chemical (DDEC) charge partitioning method is used to derive atomic site charges from electron densities. [105–110] This procedure is applied to seven compositions of [BMIM][Cl][BF_4] system. Analysis of the net ion charges (NICs) showed that the cation's (BMIM) charge varies linearly with anion composition, whereas the anion charges remain invariant. An X-ray Photoelectron Spectroscopy (XPS) study of a similar ionic liquid mixture by Licence *et al.* revealed that the N 1s binding energy of the cation varies linearly with composition, whereas that of anion remains invariant. [141] This experimental result serves as direct evidence to our findings.

Chapter 2B describes the hydrogen bond exchange process in the same binary mixture. Doseok *et al*. used IR and NMR experiments to study the hydrogen bond environment in [BMIM][Cl][BF_4]. [142] A discrepancy was observed, with IR spectra indicating two distinct hydrogen bond environments and NMR showing only one. The difference in

the time scales of IR and NMR techniques was thought of as the probable cause for this discrepancy. We estimated the time scales of exchange of hydrogen bonds between the cation and the two anions. We defined a time-dependent pair correlation function to describe this phenomenon quantitatively. The timescales of exchange were shown to be in nanoseconds which is in between the timescale of IR method (picosecond) and NMR method (microsecond), hence resolving the discrepancy.

Chapter 3 describes the validation of a force field for a new class of ionic liquids called oligomeric ionic liquids (OILs). Aida *et al.* reported that, by linking imidazolium cations via an ether linkage, double layer capacitance of devices using ILs could be improved six-fold. [65] To accurately model this class of ionic liquids, a general force field needs to be systematically refined. We used the General Amber Force Field (GAFF) force field, along with some modified parameters for ether linkage, to study this system. A representative set of gas phase conformers was created by geometry optimization in DFT framework. Atomic site charges were then refined using an iterative procedure by simultaneously fitting the electrostatic potential of multiple configurations using the restrained electrostatic potential (RESP) procedure. These charges were then used to simulate the bulk liquid and the IL-vacuum interface. Due to the sluggish behaviour of OILs, multiple independent trajectories generated by a charge scaling procedure were used to analyze the results. Density and viscosity values from simulations are found to be in good agreement with experimental values. Preliminary findings of local and interfacial structure reveal striking similarities with that of monomeric ionic liquids.

Chapter 4 summarizes the thesis and provides a brief future outlook. Interfacial structure of binary ionic liquids could be studied to investigate selective enrichment near the surface. Mesoscopic structure could be studied to examine any structural differences between monomeric and oligomeric ionic liquids.

Bibliography

[1] Welton, T. *Chem. Rev.* **1999**, *99*, 2071–2084.

[2] Hallett, J. P.; Welton, T. *Chem. Rev.* **2011**, *111*, 3508–3576.

[3] Welton, T. *Biophys. Rev.* **2018**, *10*, 691–706.

[4] Israelachvili, J. N. *Unifying Concepts in Intermolecular and Interparticle Forces*; Academic Press, 2011.

[5] Rogers, R. D.; Seddon, K. R.; Volkov, S. *Green Industrial Applications of Ionic Liquids*; Springer, 2002.

[6] Freemantle, M. *An Introduction to Ionic Liquids*; The Royal Society of Chemistry, 2009.

[7] Kirchner, B.; Clare, B. *Ionic Liquids*; Topics in Current Chemistry; 2009.

[8] Rollet, A.-L.; Bessada, C. *NMR Studies of Molten Salt and Room Temperature Ionic Liquids*; Annual Reports on NMR Spectroscopy; Academic Press, 2013.

[9] Angell, C. A.; Ansari, Y.; Zhao, Z. *Faraday Discuss.* **2012**, *154*, 9–27.

[10] Wang, H.; Gurau, G.; Rogers, R. D. *Dissolution of Biomass Using Ionic Liquids*; Springer Berlin Heidelberg, 2014.

[11] Wang, J.; Wang, H. *Aggregation in Systems of Ionic Liquids*; Springer Berlin Heidelberg, 2014.

[12] Kerscher, B.; Schüler, F.; Appel, A.-K.; Schadt, K.; Mülhaupt, R. *Nanostructured Polymeric Ionic Liquids*; Springer International Publishing, 2013.

[13] Hollóczki, O.; Nyulászi, L. *Carbenes from Ionic Liquids*; Springer Berlin Heidelberg, 2014.

[14] Eshetu, G. G.; Armand, M.; Scrosati, B.; Passerini, S. *Angew. Chem. Int. Ed.* **2014**, *53*, 13342–13359.

[15] Zhang, Q.; Shreeve, J. M. *Chem. Rev.* **2014**, *114*, 10527–10574.

[16] Ananikov, V. P. *Chem. Rev.* **2011**, *111*, 418–454.

[17] Tang, S.; Baker, G. A.; Zhao, H. *Chem. Soc. Rev.* **2012**, *41*, 4030–4066.

[18] Lei, Z.; Dai, C.; Chen, B. *Chem. Rev.* **2014**, *114*, 1289–1326.

[19] Sun, X.; Luo, H.; Dai, S. *Chem. Rev.* **2012**, *112*, 2100–2128.

[20] Osada, I.; Vries, H.; Scrosati, B.; Passerini, S. *Angew. Chem. Int. Ed.* **2016**, *55*, 500–513.

[21] Zhang, S.; Sun, J.; Zhang, X.; Xin, J.; Miao, Q.; Wang, J. *Chem. Soc. Rev.* **2014**, *43*, 7838–7869.

[22] Wang, H.; Gurau, G.; Rogers, R. D. *Chem. Soc. Rev.* **2012**, *41*, 1519–1537.

[23] Freudenmann, D.; Wolf, S.; Wolff, M.; Feldmann, C. *Angew. Chem. Int. Ed.* **2011**, *50*, 11050–11060.

[24] Werner, S.; Haumann, M.; Wasserscheid, P. *Ann. Rev. Chem. Biomol. Eng.* **2010**, *1*, 203–230.

[25] Marrucho, I.; Branco, L.; Rebelo, L. *Ann. Rev. Chem. Biomol. Eng.* **2014**, *5*, 527–546.

[26] Eshetu, G. G.; Armand, M.; Ohno, H.; Scrosati, B.; Passerini, S. *Energy Environ. Sci.* **2016**, *9*, 49–61.

[27] Jutz, F.; Andanson, J.-M.; Baiker, A. *Chem. Rev.* **2011**, *111*, 322–353.

[28] Fedorov, M. V.; Kornyshev, A. A. *Chem. Rev.* **2014**, *114*, 2978–3036.

[29] Zhang, Y.; Gao, H.; Joo, Y.-H.; Shreeve, J. M. *Angew. Chem. Int. Ed.* **2011**, *50*, 9554–9562.

[30] Jr., E. W. C.; Margulis, C. J.; Maroncelli, M.; Wishart, J. F. *Ann. Rev. Phys. Chem.* **2011**, *62*, 85–105.

[31] Xin, B.; Hao, J. *Chem. Soc. Rev.* **2014**, *43*, 7171–7187.

[32] Le Bideau, J.; Viau, L.; Vioux, A. *Chem. Soc. Rev.* **2011**, *40*, 907–925.

[33] Isambert, N.; Duque, M. d. M. S.; Plaquevent, J.-C.; Genisson, Y.; Rodriguez, J.; Constantieux, T. *Chem. Soc. Rev.* **2011**, *40*, 1347–1357.

[34] Bara, J. E.; Camper, D. E.; Gin, D. L.; Noble, R. D. *Acc. Chem. Res.* **2010**, *43*, 152–159.

[35] Lee, J. W.; Shin, J. Y.; Chun, Y. S.; Jang, H. B.; Song, C. E.; Lee, S. *Acc. Chem. Res.* **2010**, *43*, 985–994.

[36] Giernoth, R. *Angew. Chem. Int. Ed.* **2010**, *49*, 2834–2839.

[37] Hu, Y.-F.; Liu, Z.-C.; Xu, C.-M.; Zhang, X.-M. *Chem. Soc. Rev.* **2011**, *40*, 3802–3823.

[38] Greaves, T. L.; Drummond, C. J. *Chem. Soc. Rev.* **2013**, *42*, 1096–1120.

[39] Hubbard, C. D.; Illner, P.; van Eldik, R. *Chem. Soc. Rev.* **2011**, *40*, 272–290.

[40] Li, H.; Rutland, M. W.; Atkin, R. *Phys. Chem. Chem. Phys.* **2013**, *15*, 14616–14623.

[41] Volland, M.; Seitz, V.; Masse, M.; Flores, M.; Papp, R.; Massonne, K.; Stegmann, V.; Halbritter, K.; Noe, R.; Bartsch, M.; et al., Method for the separation of acids from chemical reaction mixtures by means of ionic fluids. 2003.

[42] Freyland, W. *Coulombic Fluids: Bulk and Interfaces*; Springer Series in Solid-State Sciences; 2011.

[43] Canongia Lopes, J. N.; Pádua, A. A. *J. Phys. Chem. B* **2006**, *110*, 3330–3335.

[44] Bruce, D. W.; Cabry, C. P.; Lopes, J. N.; Costen, M. L.; D'Andrea, L.; Grillo, I.; Marshall, B. C.; McKendrick, K. G.; Minton, T. K.; Purcell, S. M.; Rogers, S.; Slattery, J. M.; Shimizu, K.; Smoll, E.; Tesa-Serrate, M. A. *J. Phys. Chem. B* **2017**, *121*, 6002–6020.

[45] Hunt, P. A.; Ashworth, C. R.; Matthews, R. P. *Chem. Soc. Rev.* **2015**, *44*, 1257–1288.

[46] Dommert, F.; Schmidt, J.; Qiao, B.; Zhao, Y.; Krekeler, C.; Delle Site, L.; Berger, R.; Holm, C. *J. Chem. Phys.* **2008**, *129*, 224501.

[47] Nancarrow, P.; Mohammed, H. *ChemBioEng Reviews* **2017**, *4*, 106–119.

[48] Francesca, K.; Ray, M. *Alternative Solvents for Green Chemistry: Edition 2*; Royal Society of Chemistry, 2013.

[49] J., E. M.; R., S. K. *Pure Appl. Chem.* **2000**, *72*, 1391.

[50] Swatloski, R. P.; Spear, S. K.; Holbrey, J. D.; Rogers, R. D. *J. Am. Chem. Soc.* **2002**, *124*, 4974–4975.

[51] Payal, R. S.; Bharath, R.; Periyasamy, G.; Balasubramanian, S. *J. Phys. Chem. B* **2012**, *116*, 833–840.

[52] Payal, R. S.; Balasubramanian, S. *Phys. Chem. Chem. Phys.* **2014**, *16*, 17458–17465.

[53] Armand, M.; Endres, F.; MacFarlane, D. R.; Ohno, H.; Scrosati, B. *Nat. Mater.* **2009**, *8*, 621–629.

[54] MacFarlane, D. R.; Tachikawa, N.; Forsyth, M.; Pringle, J. M.; Howlett, P. C.; Elliott, G. D.; Davis, J. H.; Watanabe, M.; Simon, P.; Angell, C. A. *Energy Environ. Sci.* **2014**, *7*, 232–250.

[55] Hapiot, P.; Lagrost, C. *Chem. Rev.* **2008**, *108*, 2238–2264.

[56] Lin, R.; Taberna, P.-L.; Fantini, S.; Presser, V.; PÃl'rez, C. R.; Malbosc, F.; Rupesinghe, N. L.; Teo, K. B. K.; Gogotsi, Y.; Simon, P. *J. Phys. Chem. Lett.* **2011**, *2*, 2396–2401.

[57] Rehman, A.; Zeng, X. *Acc. Chem. Res.* **2012**, *45*, 1667–1677.

[58] Xu, W.; Angell, C. A. *Science* **2003**, *302*, 422–425.

[59] Greaves, T. L.; Drummond, C. J. *Chem. Rev.* **2015**, *115*, 11379–11448.

[60] Greaves, T. L.; Drummond, C. J. *Chem. Rev.* **2008**, *108*, 206–237.

[61] Noda, A.; Susan, M. A. B. H.; Kudo, K.; Mitsushima, S.; Hayamizu, K.; Watanabe, M. *J. Phys. Chem. B* **2003**, *107*, 4024–4033.

[62] Kay, J. N.; Higgins, S. J.; Jeppesen, J. O.; Leary, E.; Lycoops, J.; Ulstrup, J.; Nichols, R. J. *J. Am. Chem. Soc.* **2012**, *134*, 16817–16826.

[63] Xin, n.; Li, X.; Jia, C.; Gong, Y.; Li, M.; Wang, S.; Zhang, G.; Yang, J.; Guo, X. *Angew. Chem. Int. Ed.* **2018**, *57*, 14026–14031.

[64] Rotenberg, B.; Salanne, M. *J. Phys. Chem. Lett.* **2015**, *6*, 4978–4985.

[65] Matsumoto, M.; Shimizu, S.; Sotoike, R.; Watanabe, M.; Iwasa, Y.; Itoh, Y.; Aida, T. *J. Am. Chem. Soc.* **2017**, *139*, 16072–16075.

[66] Eftekhari, A. *Energy Storage Materials* **2017**, *9*, 47 – 69.

[67] Merlet, C.; Rotenberg, B.; Madden, P. A.; Salanne, M. *Phys. Chem. Chem. Phys.* **2013**, *15*, 15781–15792.

[68] Kirchner, K.; Kirchner, T.; Ivaništšev, V.; Fedorov, M. *Electrochim. Acta* **2013**, *110*, 762–771.

[69] Blanchard, L. a.; Hancu, D. *Nature* **1999**, *399*, 28–29.

[70] Blanchard, L. A.; Hancu, D.; Beckman, E. J.; Brennecke, J. F. *Nature* **1999**, *399*, 28–29.

[71] Cadena, C.; Anthony, J. L.; Shah, J. K.; Morrow, T. I.; Brennecke, J. F.; Maginn, E. J. *J. Am. Chem. Soc.* **2004**, *126*, 5300–5308.

[72] Anderson, J. L.; Dixon, J. K.; Maginn, E. J.; Brennecke, J. F. *J. Phys. Chem. B* **2006**, *110*, 15059–15062.

[73] Anthony, J. L.; Maginn, E. J.; Brennecke, J. F. *J. Phys. Chem. B* **2002**, *106*, 7315–7320.

[74] Bhargava, B. L.; Balasubramanian, S. *J. Phys. Chem. B* **2007**, *111*, 4477–4487.

[75] Pan, M.; Zhao, Y.; Zeng, X.; Zou, J. *Energy & Fuels* **2018**, *32*, 6130–6135.

[76] Rapaport, D. C. *The Art of Molecular Dynamics Simulation*; Cambridge University Press, 2014.

[77] Allen, M. P.; Tildesley, D. J. *Computer Simulation of Liquids*; Oxford University Press, USA, 1989.

[78] Frenkel, D.; Smit, B. *Understanding Molecular Simulation: From Algorithms to Applications*; Academic Press, Inc., 1996.

[79] Tuckerman, M. *Statistical Mechanics: Theory and Molecular Simulation*; Oxford University Press Oxford, 2010.

[80] Marx, D.; Hutter, J. *Ab Initio Molecular Dynamics : Basic Theory and Advanced Methods*; Cambridge University Press, 2009.

[81] Martin, R. M. *Electronic Structure: Basic Theory and Practical Methods (Vol 1)*; Cambridge University Press, 2004.

[82] Kohanoff, J. *Electronic Structure Calculations for Solids and Molecules: Theory and Computational Methods*; Cambridge University Press, 2006.

[83] Szabó, A.; Ostlund, N. S. *Modern quantum chemistry : introduction to advanced electronic structure theory*; Dover Publications, 1996.

[84] Capelle, K. *A bird's-eye view of density-functional theory*; cond-mat/0211443, 2002.

[85] Sholl, D.; Steckel, J. A. *Density Functional Theory: A Practical Introduction*; Wiley, 2009.

[86] Giovanni Ciccotti, I. R. M., Daan Frenkel *Simulation of liquids and solids: molecular dynamics and Monte Carlo methods in statistical mechanics*; North-Holland, 1987.

[87] Nosé, S. *J. Chem. Phys.* **1984**, *81*, 511–519.

[88] Nosé, S. *Mol. Phys.* **1984**, *52*, 255–268.

[89] Martyna, G. J.; Klein, M. L.; Tuckerman, M. *J. Chem. Phys.* **1992**, *97*, 2635–2643.

[90] Billy D. Todd, P. J. D. *Nonequilibrium Molecular Dynamics: Theory, Algorithms and Applications*; Cambridge University Press, 2017.

[91] González, M.A., *JDN* **2011**, *12*, 169–200.

[92] Guvench, O.; MacKerell, A. D. In *Molecular Modeling of Proteins*; Kukol, A., Ed.; Humana Press, 2008; pp 63–88.

[93] Schmidt, J.; Krekeler, C.; Dommert, F.; Zhao, Y.; Berger, R.; Site, L. D.; Holm, C. *J. Phys. Chem. B* **2010**, *114*, 6150–6155.

[94] Mondal, A.; Balasubramanian, S. *J. Phys. Chem. B* **2014**, *118*, 3409–3422.

[95] Shih, A. Y.; Freddolino, P. L.; Arkhipov, A.; Schulten, K. *J. Struct. Biol.* **2007**, *157*, 579 – 592, Advances in Molecular Dynamics Simulations.

[96] Kleinjung, J.; Fraternali, F. *Current Opinion in Structural Biology* **2014**, *25*, 126 – 134.

[97] Audus, D. J.; Starr, F. W.; Douglas, J. F. *Soft Matter* **2018**, *14*, 1622–1630.

[98] Perez, D.; Uberuaga, B. P.; Shim, Y.; Amar, J. G.; Voter, A. F. In *Chapter 4 Accelerated Molecular Dynamics Methods: Introduction and Recent Developments*; Wheeler, R. A., Ed.; Annual Reports in Computational Chemistry; Elsevier, 2009; Vol. 5; pp 79 – 98.

[99] Stefan, G. *J. Comput. Chem.* **2006**, *27*, 1787–1799.

[100] Bader, R. F. W.; MacDougall, P. J.; Lau, C. D. H. *J. Am. Chem. Soc.* **1984**, *106*, 1594–1605.

[101] Bayly, C. I.; Cieplak, P.; Cornell, W. D.; Kollman, P. A. *J. Phys. Chem.* **1993**, *97*, 10269–10280.

[102] Bultinck, P.; Alsenoy, C. V.; Ayers, P. W.; Carbó-Dorca, R. *J. Chem. Phys.* **2007**, *126*, 144111.

[103] Bultinck, P.; Cooper, D. L.; Dimitri, V. N. *Phys. Chem. Chem. Phys.* **2009**, *11*, 3424–3429.

[104] Reed, A. E.; Weinstock, R. B.; Weinhold, F. *J. Chem. Phys.* **1985**, *83*, 735–746.

[105] Manz, T. A.; Sholl, D. S. *J. Chem. Theory Comput.* **2010**, *6*, 2455–2468.

[106] Manz, T. A.; Sholl, D. S. *J. Chem. Theory Comput.* **2012**, *8*, 2844–2867.

[107] Manz, T. A.; Limas, N. G. *RSC Adv.* **2016**, *6*, 47771–47801.

[108] Limas, N. G.; Manz, T. A. *RSC Adv.* **2016**, *6*, 45727–45747.

[109] Manz, T. A. *RSC Adv.* **2017**, *7*, 45552–45581.

[110] Limas, N. G.; Manz, T. A. *RSC Adv.* **2018**, *8*, 2678–2707.

[111] Nazarian, D.; Camp, J. S.; Sholl, D. S. *Chem. Mater.* **2016**, *28*, 785–793.

[112] Mondal, A.; Balasubramanian, S. *J. Phys. Chem. B* **2015**, *119*, 11041–11051.

[113] Dong, K.; Liu, X.; Dong, H.; Zhang, X.; Zhang, S. *Chemical Reviews* **2017**, *117*, 6636–6695.

[114] Kirchner, B.; Hollóczki, O.; Lopes, J. N. C.; Pádua, A. A. H. *WIREs. Comput. Mol. Sci.* **2015**, *5*, 202–214.

[115] Dommert, F.; Wendler, K.; Berger, R.; Delle Site, L.; Holm, C. *ChemPhysChem* **2012**, *13*, 1625–1637.

[116] Canongia Lopes, J. N.; Deschamps, J.; Pádua, A. A. *J. Phys. Chem. B* **2004**, *108*, 2038–2047.

[117] Lopes, C. J. N.; Deschamps, J.; Pádua, A. A. *J. Phys. Chem. B* **2004**, *108*, 11250–11250.

[118] Canongia Lopes, J. N.; Pádua, A. A. *J. Phys. Chem. B* **2004**, *108*, 16893–16898.

[119] Canongia Lopes, J. N.; Pádua, A. A. *J. Phys. Chem. B* **2006**, *110*, 19586–19592.

[120] Canongia Lopes, J. N.; Pádua, A. A.; Shimizu, K. *J. Phys. Chem. B* **2008**, *112*, 5039–5046.

[121] Wang, J.; Wolf, R. M.; Caldwell, J. W.; Kollman, P. A.; Case, D. A. *J. Comput. Chem.* **2004**, *25*, 1157–1174.

[122] Jorgensen, W. L.; Maxwell, D. S.; Tirado-Rives, J. *J. Am. Chem. Soc.* **1996**, *118*, 11225–11236.

[123] Sambasivarao, S. V.; Acevedo, O. *J. Chem. Theory Comput.* **2009**, *5*, 1038–1050.

[124] Triolo, A.; Russina, O.; Bleif, H.-J.; Cola, E. D. *J. Phys. Chem. B* **2007**, *111*, 4641–4644.

[125] Wendler, K.; Dommert, F.; Zhao, Y. Y.; Berger, R.; Holm, C.; Delle Site, L. *Faraday Discuss.* **2012**, *154*, 111–132.

[126] Florian, D.; Christian, H. *Phys. Chem. Chem. Phys.* **2013**, *15*, 2037–2049.

[127] Zhang, Y.; Maginn, E. J. *J. Phys. Chem. B* **2012**, *116*, 10036–10048.

[128] Skarmoutsos, I.; Welton, T.; Hunt, P. A. *Phys. Chem. Chem. Phys.* **2014**, *16*, 3675–3685.

[129] Thar, J.; Brehmy, M.; Seitsonen, A. P.; Kirchner, B. *J. Phys. Chem. B* **2009**, *113*, 15129–15132.

[130] Lian, C.; Su, H.; Liu, H.; Wu, J. *J. Phys. Chem. C* **2018**, *122*, 14402–14407.

[131] Plimpton, S. *J. Comput. Phys.* **1995**, *117*, 1–19.

[132] Brown, W. M.; Peng, W.; Plimpton, S. J.; Tharrington, A. N. *Comput. Phys. Commun.* **2011**, *182*, 898–911.

[133] Brown, W. M.; Kohlmeyer, A.; Plimpton, S. J.; Tharrington, A. N. *Comput. Phys. Commun.* **2012**, *183*, 449–459.

[134] Dennington, R.; Keith, T.; Millam, J. GaussView Version 5. Semichem Inc., Shawnee Mission, KS, 2009.

[135] Frisch, M. J. et al. Gaussian 09 Revision D.01. Gaussian Inc. Wallingford CT **2009**.

[136] Martinez, L.; Andrade, R.; Birgin, E. G.; Martinez, J. M. *J. Comput. Chem.* **2009**, *30*, 2157–2164.

[137] Hutter, J.; Iannuzzi, M.; Schiffmann, F.; VandeVondele, J. *WIREs Comput. Mol. Sci.* **2014**, *4*, 15–25.

[138] Wang, J.; Wang, W.; Kollman, P. A.; A., C. D. *J. Mol. Graph. Model.* **2006**, *25*, 247–260.

[139] Dupradeau, F.-Y.; Pigache, A.; Zaffran, T.; Savineau, C.; Lelong, R.; Grivel, N.; Lelong, D.; Rosanski, W.; Cieplak, P. *Phys. Chem. Chem. Phys.* **2010**, *12*, 7821–7839.

[140] Humphrey, W.; Dalke, A.; Schulten, K. *J. Mol. Graphics* **1996**, *14*, 33–38.

[141] Villar-Garcia, I. J.; Lovelock, K. R. J.; Men, S.; Licence, P. *Chem. Sci.* **2014**, *5*, 2573–2579.

[142] Cha, S.; Kim, D. *Phys. Chem. Chem. Phys.* **2015**, *17*, 29786–29792.

Chapter 2A

Charge Environment in Binary Ionic Liquid Mixtures

Room temperature ionic liquids (RTILs) offer a wide choice of properties for their use as either solvents or electrolytes by allowing for the possibility of mixing different ionic components [1–3]. However, the compositional space of ILs is too large to be explored by experiments alone. Computer simulations play an essential role complementing experiments as well as offering insights into the microscopic behaviour of ILs [4–7].

In this regard, empirical force field (FF) based Molecular Dynamics (MD) simulations are apt, as they can offer microscopic insights as well as provide estimates of bulk/interfacial properties while using a modest amount of computational resource [8–12]. However, the reliability of MD simulations is contingent upon the fidelity of the force field [13–15]. Researchers have recognized the need to take into account charge transfer and polarizability effects between the ions in the condensed phase, for a quantitative comparison between the modelled system and experiment [16, 17]. A crucial outcome of inter-ion charge transfer is the reduction in their formal charges from unity [18]. Polarizable force fields account for

Reprinted with permission from "Charge Environment and Hydrogen Bond Dynamics in Binary Ionic Liquid Mixtures: A Computational Study" *J. Phys. Chem. Lett.* **2018**, *9*, 3511–3516. © 2018, American Chemical Society, http://pubs.acs.org/doi/abs/10.1021/acs.jpclett.8b01481.

these phenomena explicitly, and hence are more "physical" than non-polarizable ones. But this additional detail often comes at an increased computational cost [19, 20].

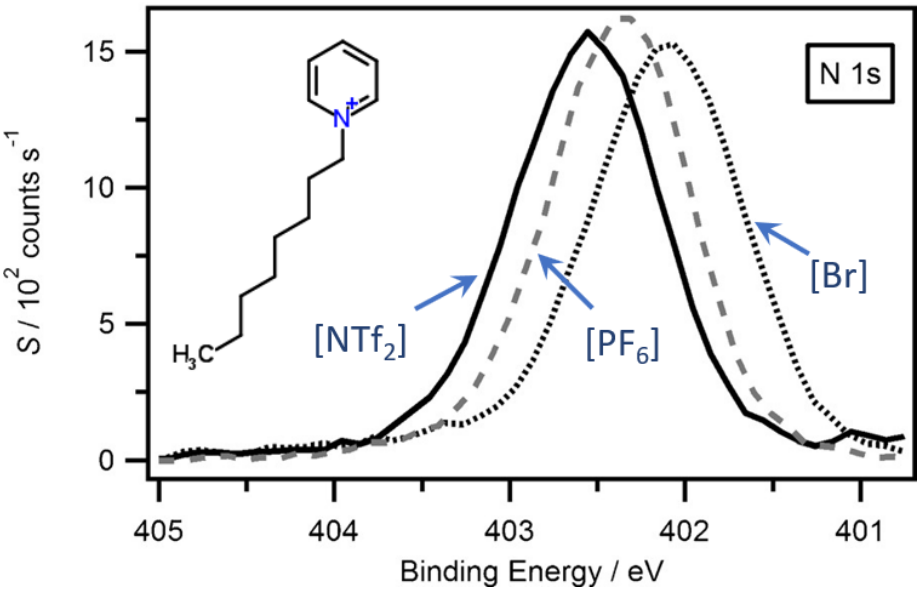

Figure 2A.1: X-ray photoelectron spectra of N 1s for the pyridinium cation ($[C_8Py]$) in three different pure ionic liquids $[C_8Py][NTF_2]$, $[C_8Py][PF_6]$ and $[C_8Py][Br]$, taken from the work of Licence et al. [21]

Although non-polarizable force fields do not account for polarization explicitly, fixed partial charges, if chosen appropriately, can capture the effects of ion polarization in a mean field manner [22]. Studies have shown that some structural (like X-ray structure factor) [23, 24] and dynamical properties (like diffusion constants) [25] are most affected by the choice of partial charges, hence it is imperative that they are parametrized consistently.

In one study, Licence *et al.* investigated various pure ionic liquids with pyridinium cation and three different anions ($[C_8Py][A]$, where A = $[NTF_2]$ or $[PF_6]$ or [Br] anions) using XPS. [21] Figure 2A.1 shows the cation's N 1s binding energy peaks in three different pure ionic liquids $[C_8Py][NTF_2]$, $[C_8Py][PF_6]$ and $[C_8Py][Br]$. Both N 1s and C 1s binding energies of the cation show clear trend – $[NTF_2] > [PF_6] > [Br]$. Moreover, as the cation binding energy is positively correlated (a higher binding energy implies more electropositive cation) to the electrospositivity of the cation, they conclude that more basic anions transfer more of its charge to cations. For example, [Br] being the most basic anion (among the three) donates most amount of charge to the cation, making it less electropostive as

evidenced by the low binding energy.

As the extent of charge transfer between the cation and the anion can depend on their type, a non-polarizable force field based on fixed ion charges (sub-unity) will need to be transferable to mixtures, i.e., ionic liquids which contain one type of cation and two different types of anions (say). Addressing this problem, using periodic quantum density functional theory (DFT) calculations, we demonstrate the linear variation of cation charge with anion composition, a result which segues with results from X-ray photoelectron spectroscopy (XPS). [26] This observation constitutes the basis on which a linear charge mixing approach can be adopted within a force field. MD simulations, using such a force field, reproduce experimental data on IL mixtures and throw considerable light on the microscopic exchange mechanisms of anion types in the coordination shell of a cation. These studies are pursued in a binary ionic liquid (BIL) system with 1-butyl-3-methylimidazolium [BMIM] as the common cation and chloride [Cl] and tetrafluoroborate [BF_4] as the counter anions [27].

2A.1 Methodology and Computational Details

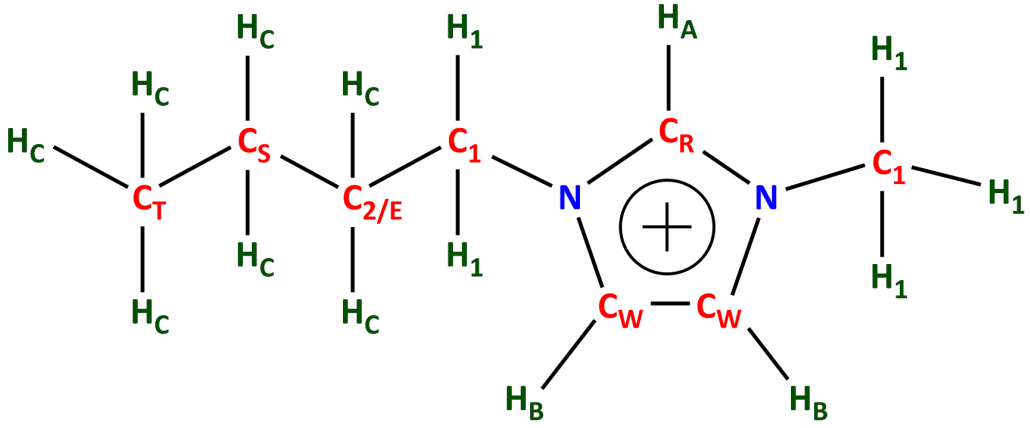

Figure 2A.2: Molecular structure of 1-butyl-3-methylimidazolium cation.

All the binary ionic liquid mixtures considered in this study have one common cation and two kinds of anions. In the case of [BMIM][Cl]$_x$[BF_4]$_{1-x}$, the composition of mixtures is expressed in terms of mole fraction (number of [Cl]/total number of anions) of [Cl] anion and in the case of [BMIM][NTf_2]$_x$[SCN]$_{1-x}$, the composition is expressed in terms of mole fraction of [NTf_2] anion. Tables 2A.1 and 2A.2 list the compositions and the corresponding

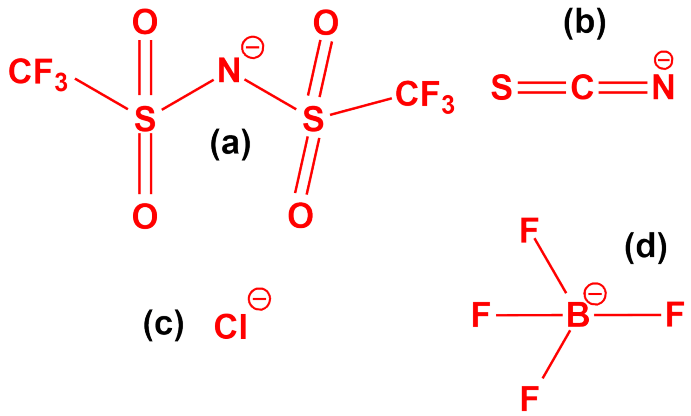

Figure 2A.3: Molecular structures of (a) [NTf_2], (b) [SCN], (c) [Cl], (d) [BF_4] anions.

Table 2A.1: Compositions and simulation box size for [BMIM][Cl]$_x$[BF_4]$_{1-x}$ system.

Composition (x)	Small systems		Large systems	
	Number of ion pairs	Box size (Å)	Number of ion pairs	Box size (Å)
0.00	28	20.69	512	54.19
0.25	28	20.49	512	53.62
0.40	28	20.34	512	53.27
0.50	28	20.23	512	53.01
0.60	28	20.14	512	52.74
0.75	28	20.02	512	52.38
1.00	28	20.01	512	51.74

size of the systems considered. A schematic representation of [BMIM] ion along with the atom labels is shown Figure 2A.2 to aid further discussion.

Table 2A.2: Compositions and simulation box size for [BMIM][NTf_2]$_x$[SCN]$_{1-x}$ system.

Composition (x)	Large systems	
	Number of ion pairs	Box size (Å)
0.00	512	53.94
0.25	512	56.20
0.50	512	58.54
0.75	512	60.69
1.00	512	62.84

2A.1.1 Atomic site charges

Figure 2A.4 summarizes the procedure used to derive atomic site charges of any Ionic Liquid (IL) system considered in this study. Most of the binary ionic liquids (BILs) studied

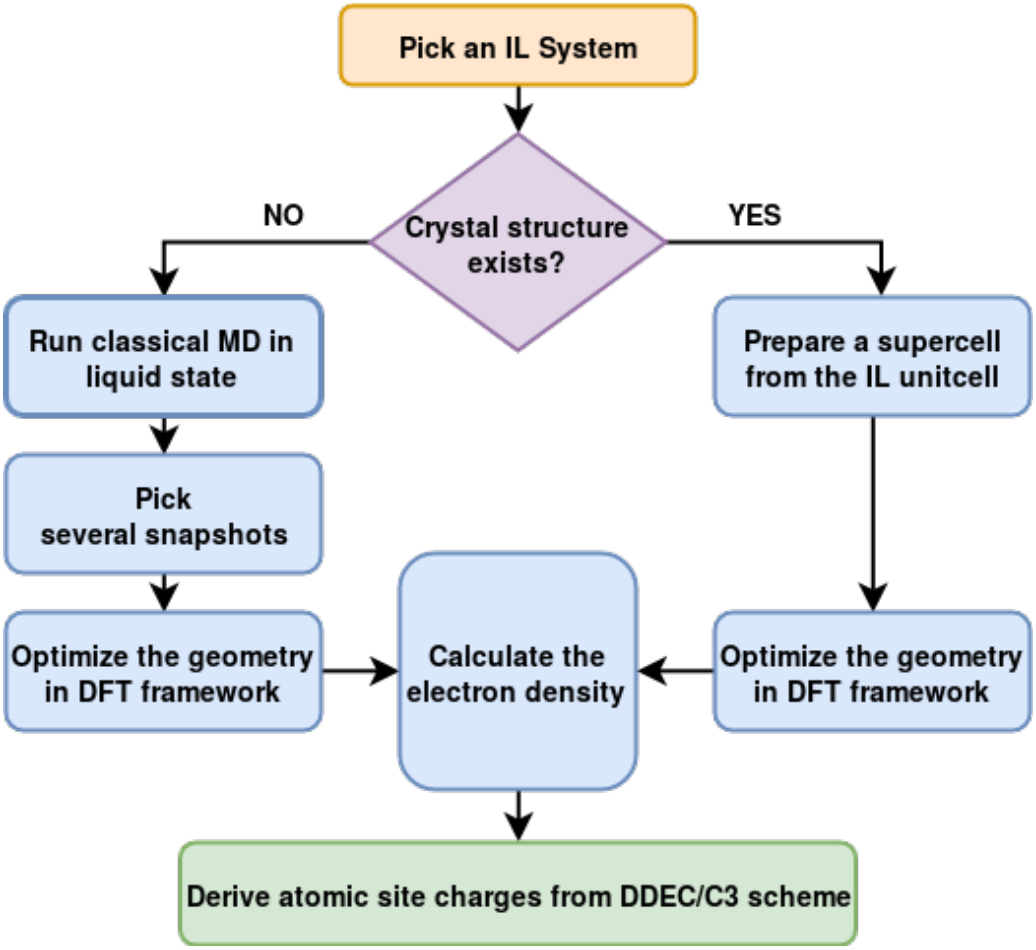

Figure 2A.4: Flow chart illustrating the procedure to derive atomic site charges.

till now exist in liquid state at ambient conditions [28]. Moreover, crystal phases of BILs have not yet been reported. Hence we derived the atomic site charges of BILs from quantum DFT calculations of a few representative liquid snapshots. These snapshots themselves were selected from classical molecular dynamics trajectories of the liquid phase. These trajectories were generated as follows: for each composition, liquid configurations containing 28 ion pairs were created using PACKMOL package. Subsequently, an isothermal-isobaric (NPT) equilibration run was carried out at 300K and 1 atm for 10 ns. This was followed by a long isothermal NVT run of 15ns. Liquid snapshots were taken every 1ns from the last 10ns of the NVT simulation.

Table 2A.3: Lennard-Jones parameters of the Mondal-Balasubramanian (MB) force field [29, 30].

Atom	ϵ (KJ mol^{-1})	σ (Å)
N	0.71128	3.25
C_R	0.29288	3.55
C_W	0.29288	3.55
H_A	0.04184	1.70
H_B	0.12552	2.00
C_1	0.27614	3.50
H_1	0.12552	2.50
C_2	0.27614	3.50
H_C	0.12552	2.50
C_S	0.27614	3.50
C_T	0.27614	3.50

Table 2A.4: Atomic site charges of the cation atoms in pure IL systems, containing any of the four anions considered here as reported in the MB force field [29, 30].

Atom	Charge (e)			
	$[Cl]$	$[BF_4]$	$[NTf_2]$	$[SCN]$
N	0.130	0.140	0.145	0.120
C_R	-0.010	-0.010	-0.005	-0.005
C_W	-0.130	-0.110	-0.120	-0.110
H_A	0.150	0.180	0.175	0.145
H_B	0.140	0.170	0.170	0.135
C_1	-0.250	-0.250	-0.250	-0.250
H_1	0.120	0.120	0.120	0.120
C_2	-0.076	-0.076	-0.076	-0.076
H_C	0.098	0.098	0.098	0.098
C_S	-0.196	-0.196	-0.196	-0.196
C_T	-0.294	-0.294	-0.294	-0.294

Table 2A.5: Atomic site charges of anion atoms as reported in the MB force field [29, 30].

Anion	Total ion charge (e)	Atom	Atomic site charge (e)
[Cl]	-0.64	Cl	-0.640
[BF_4]	-0.79	B	1.010
		F	-0.450
[NTf_2]	-0.78	N	-0.740
		S	1.090
		O	-0.545
		C	0.445
		F	-0.155
[SCN]	-0.65	S	-0.380
		C	0.260
		N	-0.530

$$
\begin{aligned}
U = & \sum_{bonds} k_b(r - r_0)^2 \\
& + \sum_{angles} k_\theta(\theta - \theta_0)^2 \\
& + \sum_{dihedrals} \sum_{n=1}^{5} A_n cos^{n-1}(\phi) \\
& + \sum_{impropers} k_i(1 + dcos(n\phi)) \\
& + \sum_i \sum_j 4\epsilon_{ij} \left[\left(\frac{\sigma_{ij}}{r_{ij}} \right)^{12} - \left(\frac{\sigma_{ij}}{r_{ij}} \right)^{6} \right] + \frac{1}{4\pi\epsilon_0} \frac{q_i q_j}{r_{ij}}
\end{aligned}
\tag{2A.1}
$$

Force field The force field parameters used for the small system MD simulations were taken from Mondal and Balasubramanian's work (MB force field) [29, 30]. The functional form of the force field, shown in equation 2A.1 is the same as the OPLS-AA force field [31, 32]. Tables 2A.3, 2A.4 and 2A.5 lists the non-bonded force field parameters used in this study for the sake of completeness. The non-bonded LJ and Coulomb interactions were scaled by 0.5 and 0.0 respectively for atoms separated by 3 bonds. The LJ cross interactions between two different atom types were obtained using Lorentz-Berthelot mixing rule.

Since the total charge on the anion depends on its type, the atomic site charges of cation atoms were weighted according to the mole fraction of the respective anion in the mixture

to maintain charge neutrality. The anion charges were taken from the corresponding pure systems. For example, say e_c represents the charge of cation (and also the anion to maintain overall charge neutrality) in the pure [BMIM][Cl] system and e_b represents the charge of cation in the pure [BMIM][BF_4] system. The cation charge in a 0.50 mole fraction BIL is taken to be $0.50 * e_c + 0.50 * e_b$. And both the anions retain the same charge of their corresponding pure systems. We call this the linear mixing rule.

In order to check for the possible effects of force field parameters on the final atomic site charges (derived using the procedure listed in Figure 2A.4), we repeated the liquid simulations using the well established CL&P force field [33–37] as well. In the CL&P force field framework, all the ions have a charge of $+1$ or -1 independent of the choice of counterion. As CL&P force field cannot incorporate linear charge mixing, these simulations should indicate if there is any force field dependence on the final results. Anticipating the results, **Figure 2A.5 demonstrates no such dependence on the force field.**

The molecular dynamics simulations were run using the LAMMPS package. [38–40] All the simulations were performed at 300K temperature. The equations of motion were integrated using velocity Verlet integrator with 1 fs timestep. All C*-H* bonds were constrained using the SHAKE algorithm. [41] particle-particle particle-mesh (PPPM) solver with a accuracy of 10^{-5} was used to calculate long range Coulombic interactions. Nosé-Hoover thermostat and barostat were used for the corresponding NVT and NPT runs. [42–44] Cubic boundary conditions were applied to simulate bulk-like environment.

DFT Calculations First, a coarse geometry optimization (gradient on nuclei converged to 0.005 a.u.) was performed on the liquid snapshots of 28 ions pairs. Triple-ζ double-polarized basis set and a density cutoff of 280 Ry was used. The Perdew, Burke and Ernzerhof (PBE) functional [45] was used to treat exchange-correlation and Grimme's D2 correction was used for dispersion correction [46]. The effect of core electrons and nuclei was represented by Geodecker-Teter-Hutter (GTH) pseudopotentials [47]. Convergence criteria of 10^{-7} for the gradient of wave function and 10^{-3} for the force on nuclei were used. All the DFT calculations were performed using CP2K package [48]. The electron

density of the final configuration, obtained after geometry optimization procedure, was used to calculate the atomic site charges using the $DDEC/c3$ scheme [49, 50]. The detailed exposition of this framework can be found elsewhere [29, 30].

2A.1.2 Force field verification for binary ionic liquids

Classical molecular dynamics simulations were performed to estimate the equilibrium properties of [BMIM][Cl]$_x$[BF$_4$]$_{1-x}$ at seven different compositions (mentioned in system description). Liquid configurations of 512 ion pairs were created using PACKMOL package [51]. After an energy minimization in the force field framework, an NPT simulation is run for 10ns at 300K and 1 atm. The last 5 ns of the trajectory was used to determine the equilibrium density. New liquid configurations of 512 ion pairs were created at the equilibrium density. These configurations were equilibrated for 5 ns in NVT ensemble at 300 K. Finally, a production run of 25 ns in the NVT ensemble followed. Three different sets of simulations were performed, each with different force field parameters. The first set uses force field parameters from Mondal-Balasubramanian (MB) [29, 30], while second (CL&P 1.0) and the third (CL&P 0.8) sets use CL&P force field parameters with atomic site charges scaled by a factor of 1.0 and 0.8 respectively. In each case, the atomic site charges of cation atoms were obtained from linear rule of mixing (see Force field topic in Section 2A.1) and anion atom charges were retained from the corresponding pure systems (Note that the atomic site charges of the pure systems were derived from DFT calculations of smaller (≈ 30 ion pairs) liquid configurations).

2A.2 Results and Discussion

2A.2.1 Charge environment

The condensed phase electronic charge density was estimated by DFT calculations of a representative set of snapshots of each BIL mixture. These snapshots were selected from classical MD trajectories of BILs generated from two different force fields. Details of these calculations are presented in Section 2A.1.1. The electron density was used to calculate the

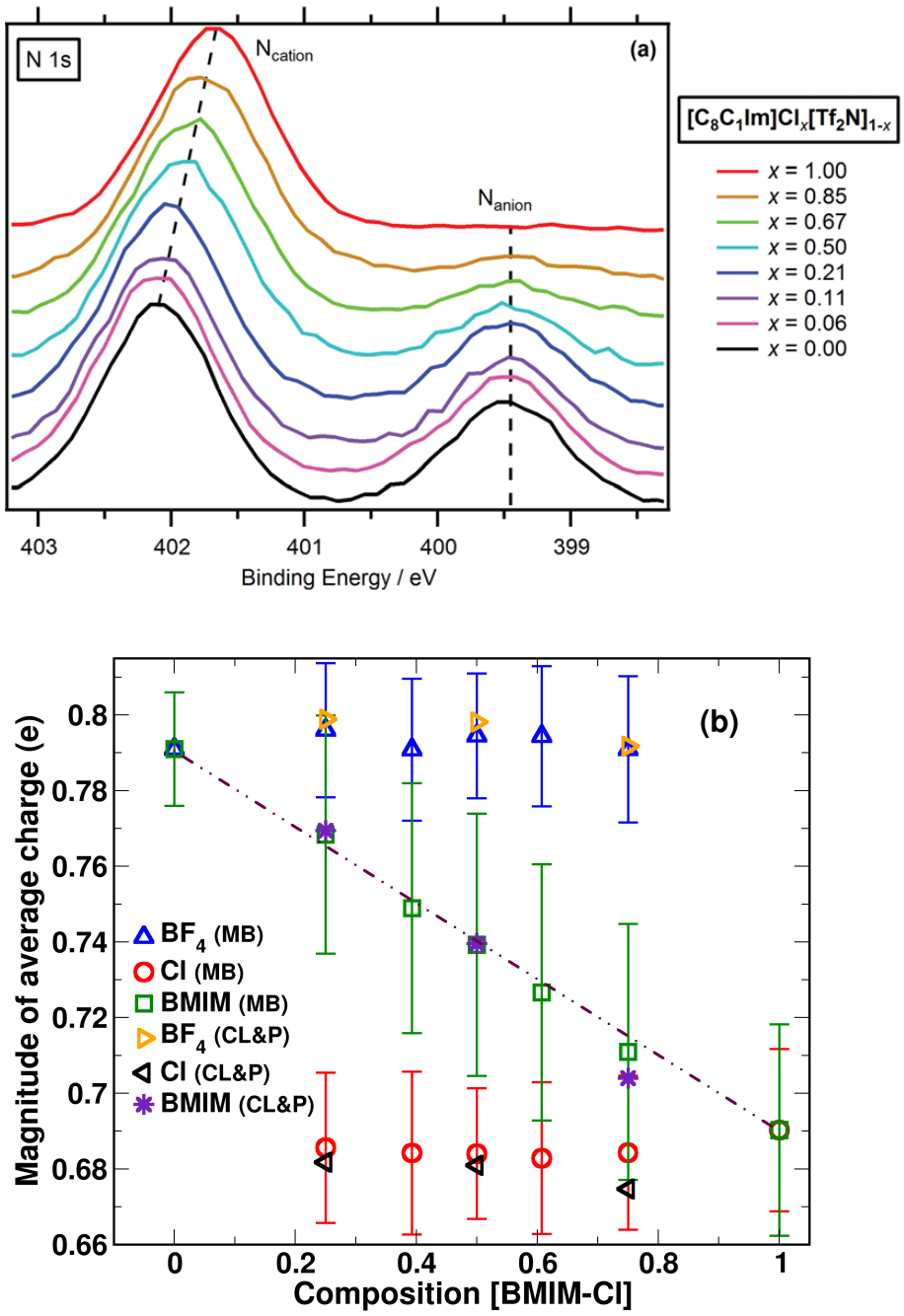

Figure 2A.5: (a) High resolution N1s XPS spectra of $[OMIM][Cl]_x[NTf_2]_{1-x}$ mixture at different compositions, taken from the work of Licence et al.[26] and (b) magnitude of average Net Ion Charges (NICs) of BMIM, [Cl] and $[BF_4]$ ions vs composition obtained from simulations. The labels indicate the ions and the corresponding force fields used to derive the NICs – (i) MB force field [29, 30] and (ii) CL&P force field [33–37]

atomic site charges using the $DDEC/c3$ method [49, 50] and the Net Ionic Charge (NIC) was obtained as the sum of atomic site charges of all atoms of an ion. Figure 2A.5 (b) shows

the variation of average NIC of [BMIM], [Cl] and [BF_4] ions with respect to composition of the BIL mixture. The average NIC of cations varies linearly between the values of the pure components, irrespective of the force field employed. In contrast, the average NICs of both the anions remain unchanged with composition. Recently, Licence et al. investigated the charge environment of ions in IL mixtures using N1s X-ray photoelectron spectroscopy [26]. Figure 2A.5 (a) shows the N1s XP spectra of [OMIM][Cl]$_x$[NTf_2]$_{1-x}$ system, which contains nitrogen in both the cation as well as in the [NTf_2] anion. The XPS measurements revealed that the binding energy of nitrogen atom in cation varied "quasi-linearly" with anion composition whereas that in the [NTf_2] anion remained unchanged. Moreover, the binding energies of all the carbon and nitrogen atoms in the cation varied quasi-linearly. Various studies have shown that the cation charge is largely centred on the ring and is independent of the alkyl tail length [29, 52, 53]. In general, the XPS binding energies of most atoms (including carbon and nitrogen) are linearly correlated to the partial charge on the atoms [54]. This would mean that the atomic partial charges of cation atoms, derived from XPS binding energies, would also vary quasi-linearly with composition. This observation serves as a direct experimental evidence to the linear variation of NIC obtained in our simulations.

In order to understand the origin of the linear trend of cation charge with anion mole fraction, we examined the local environment of cations in the BIL at 50:50 anion composition. The average NIC of cation at this composition is +0.74 a.u. We first selected two sets of cations – low charge (NIC values less than +0.70 a.u) and high charge (NIC values greater than +0.78 a.u) cations. We then determined the partial coordination number for cations belonging to each of these two sets separately.

Figure 2A.6 shows the probability density of a cation (in the 50:50 mixture) to have a certain coordination number of [Cl] and [BF_4] anions. The average number (shown as green vertical line) of [Cl] ions in the first coordination shell of a cation is higher for the low charge cations and lower for a cation with high charge. More the number of chloride ions surrounding a cation, more is the extent of charge transfer and hence lower is that cation's

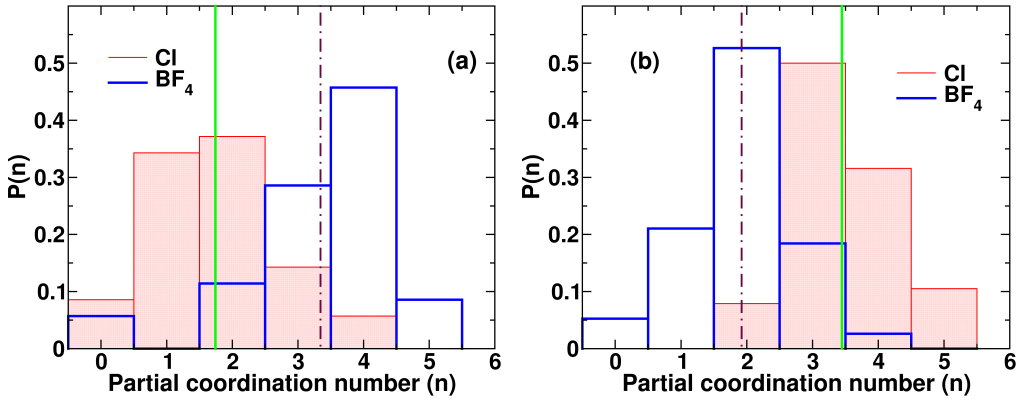

Figure 2A.6: Probability density vs partial coordination number of (a) high charge cations (charge greater than +0.78e) and (b) low charge cations (charge less than +0.70e), in a BIL with 50:50 composition. The green vertical line indicates the average partial Cl coordination number(average number of [Cl] ions surrounding a cation) and maroon dash-dot line represents the average partial [BF_4] coordination number.

NIC. This analysis clearly shows that the NIC of a cation is affected by both the number and composition of the anions surrounding it. This correlation can be used to rationalize the linear trends in average NIC of cation (Figure 2A.5). The average NIC of cations depends on the composition of their first solvation shell and which in turn depends on the bulk composition of the mixture (assuming homogeneous mixing. See Ref. [55]). These results encouraged us to adopt a linear charge mixing scheme for the ion charges modelled via classical MD simulations. While the charges of the anions are chosen to be independent of the anion composition of the IL, that of the cation is chosen as the weighted sum of the charges of the cations used in the pure systems – the weight being the mole fraction of the individual anions present in the mixture. In a liquid modeled with a polarizable force field or one with a fluctuating charge model, the charge on a specific cation would be dependent on its environment. The linear charge mixing scheme employed by us here can be viewed as a mean field approximation to such models which include explicit polarizability [20].

2A.2.2 Force field validation

Figure 2A.7a shows the variation of density with respect to composition for the [BMIM][Cl]$_x$[BF_4]$_{1-x}$ system. Results from all the three force fields show a linear trend,

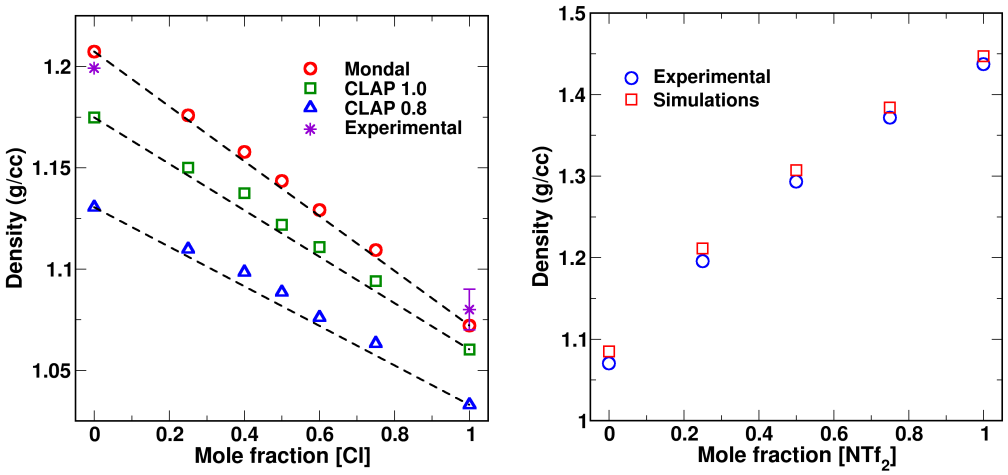

Figure 2A.7: Plots of mass density vs composition for (a) $[BMIM][Cl]_x[BF_4]_{1-x}$ system and (b) $[BMIM][NTf_2]_x[SCN]_{1-x}$ system. Error bars are not shown for data points for which symbols are larger than their standard deviation values. Dashed lines connecting the end points are drawn as guide to the eye. Experimental data obtained from Refs [56–58].

indicating the mixture to be ideal. Due to the lack of experimental data for this system at all compositions, a comparison with experiments could not be made. To gauge the efficacy of the linear charge mixing rule, we have also simulated the liquid $[BMIM][NTf_2]_x[SCN]_{1-x}$ system, for which experimental data was available (see Figure 2A.7b). For this system, simulations were carried out using the Mondal-Balasubramanian (MB) force field with linear charge mixing rule. Both experiments and simulations show a linear trend indicating the mixture to be ideal, consistent with most IL mixtures [28].

2A.2.3 Local structure

Radial distribution functions

Figure 2A.8 shows that the cation's solvation shell radius (taken as first RDF minimum) remains constant with composition. However, the amplitude of the peaks increase/decrease monotonically with composition. In the case of [Cl] ions, the amplitude of the first peak increases with decreasing [Cl] concentration while that of the second peak decreases with decreasing [Cl] concentration. The first peak arises from [Cl] ions hydrogen bonded either with H_A or with H_B atoms of the cation, while the shoulder at around 5.8 Å arises

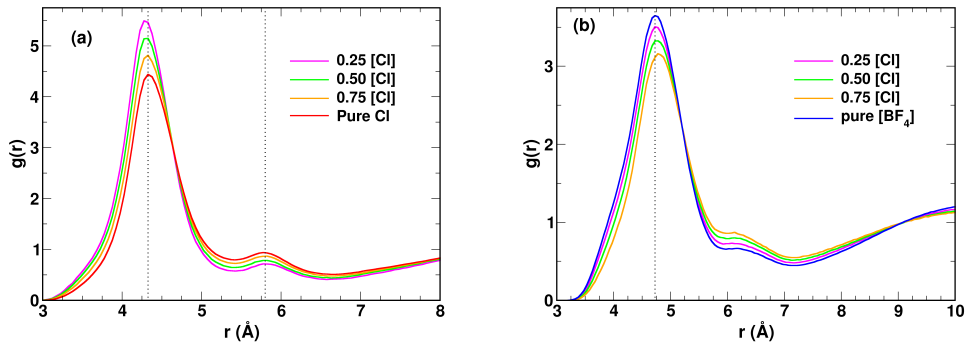

Figure 2A.8: Plots of radial distribution function of (a) cation ring center with [Cl] and (b) cation ring center with $[BF_4]$ ion (B atom). Dotted lines show the position of the peaks in the respective pure systems.

from chloride ions present in the direction of the methyl group of the cation. [8, 59] This observation means that [Cl] ions are populating the first solvation shell at the expense of the second solvation shell, as the [Cl] concentration decreases. [Cl] ions prefer to crowd near the hydrogen bonding sites of the cation (see SDF section). Hence there is a competition among [Cl] ions to occupy the best positions in the first solvation shell. As the [Cl] concentration decreases, [Cl] ions face less competition among themselves for the best interaction sites and hence migrate from second solvation shell to the first. We see an exact opposite trend in the case of [BF_4] ions. This is to be expected, as [Cl] ions are known to have stronger interaction with cation than [BF_4] ions. Hence [Cl] ions displace [BF_4] ions from the first solvation shell to the second. Although [Cl] ions are the preferred anions to interact with cations, they do not completely displace the [BF_4] ions, the effect is only little. These results are in agreement with previous findings. [55]

Spatial distribution functions (SDF)

SDF plots indicate crowding of anions of both types (Cl and BF_4) near the hydrogen bonding sites of cation (H_A and H_B). Though [Cl] ions show higher propensity than [BF_4] ions (see RDF plots), they do not displace [BF_4] ions from their interaction sites. This serves as an evidence that [BF_4] ions can participate in hydrogen bonding. It must also be noted that the SDF shows the average solvation shell picture, so the presence of both

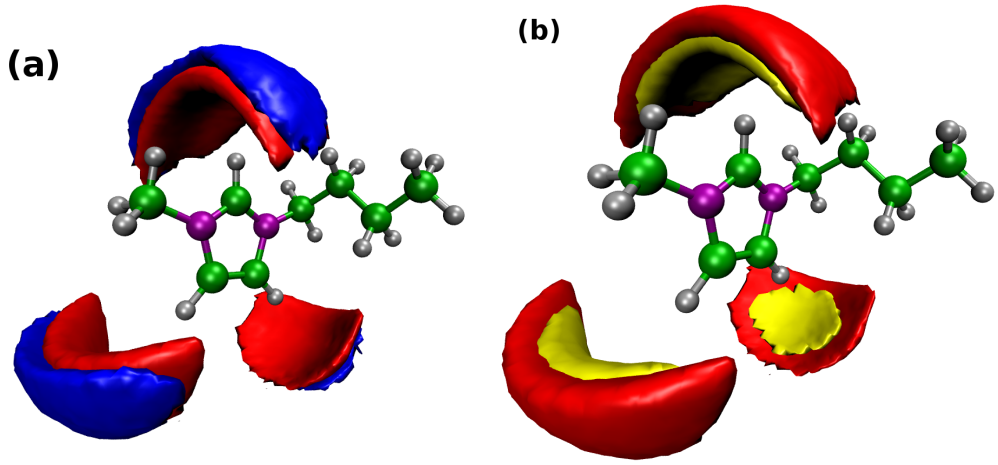

Figure 2A.9: Isosurfaces of spatial distribution function of (a) Cl and B atoms around cation and (b) Cl and F atoms around cation, of 50:50 BIL mixture. Isosurface color index – Red : Cl atom, Blue : B atom and Yellow : F atom. Cation atom color index – Silver : H, Green : C, Purple : N. Isosurface value of Cl and B atoms at 0.01675 $Å^{-3}$, F atoms at 0.04321 $Å^{-3}$.

[Cl] and [BF_4] densities at one location does not imply that both ions are present in every cation's solvation shell.

2A.2.4 Mean Squared Displacement

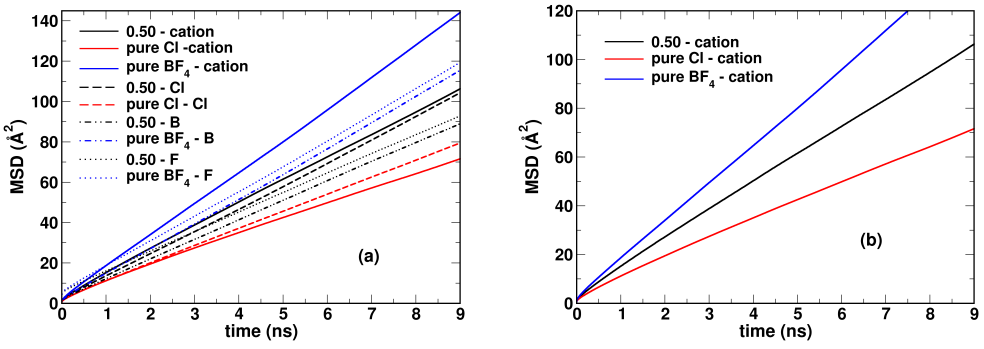

Figure 2A.10: Mean squared displacement of (a) all ions and (b) cation ring center.

MSD plots (Figure 2A.10, 2A.11) show that the cation diffuses faster than either of the anions in the 50:50 mixture of [BMIM][Cl][BF_4]. And [Cl] being lighter than the [BF_4] ion, diffuses faster among the two anions. Not unexpectedly and in line with experiments,

the dynamics in pure [BMIM][Cl] is slower than pure [BMIM][BF_4]. [BMIM][Cl] has a higher melting point (339K) than [BMIM][BF_4]. Moreover, the simulations were run at 300K and hence [BMIM][Cl] can be considered to be in a supercooled liquid state.

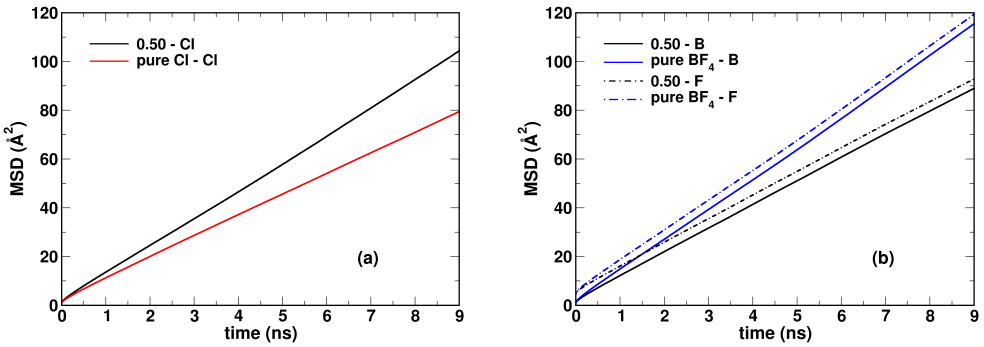

Figure 2A.11: Plots of mean squared displacement of (a) $[Cl]$ and (b) $[BF_4]$ ion (B and F atoms).

2A.3 Conclusions

Periodic DFT calculations were performed on liquid snapshots of [BMIM][Cl]$_x$[BF_4]$_{1-x}$ mixtures for which no known crystal structures exist. Atomic site charges were then derived for each composition of the mixture using the DDEC scheme. [49, 50] The net ionic charge of the cation varies linearly w.r.t composition whereas those of the anions remain the same as in their pure ILs. Dependence of the net ionic charges on the force field used to carry out the BIL MD simulations was also investigated. We have demonstrated that the charges derived are independent of the initial force field used. We call this linear dependence of cation charge and invariant anion charge as linear mixing rule.

Licence et al. showed that binary ionic liquid mixtures can be used to tune the electronic environment of the ions involved. [26] They found that the XPS binding energies of the cation atoms varies “quasi-linearly” with composition, a result which serves as an evidence for our observed linear trend in atomic site charges. We have found that the charge of a specific cation is directly correlated to the composition of its first coordination shell– Greater the fraction of more basic anions, lower is the cation charge. The agreement of our

findings with experiments gives credence to our framework to obtain condensed phase site charges. We propose a linear charge mixing scheme to obtain the atomic site charges for MD simulations of BIL mixtures.

We have demonstrated the fidelity of the MB force field to reproduce experimental data while incorporating charges obtained by linear mixing rule. Local structure of $[BMIM][Cl]_x[BF_4]_{1-x}$ mixtures shows that the solvation shell structure of the cation is retained in the mixtures with [Cl] ions showing higher propensity to interact with cations than $[BF_4]$ ions. These observations are consistent with previous findings. [28, 55]

Hydrogen bonding in imidazolium based ionic liquids is a major factor dictating the local structure of the ionic liquids. Moreover hydrogen bonding network is shown to have a direct impact on the viscosity of the ILs. Understanding the hydrogen bonding in BILs constitutes our endeavour for the next chapter.

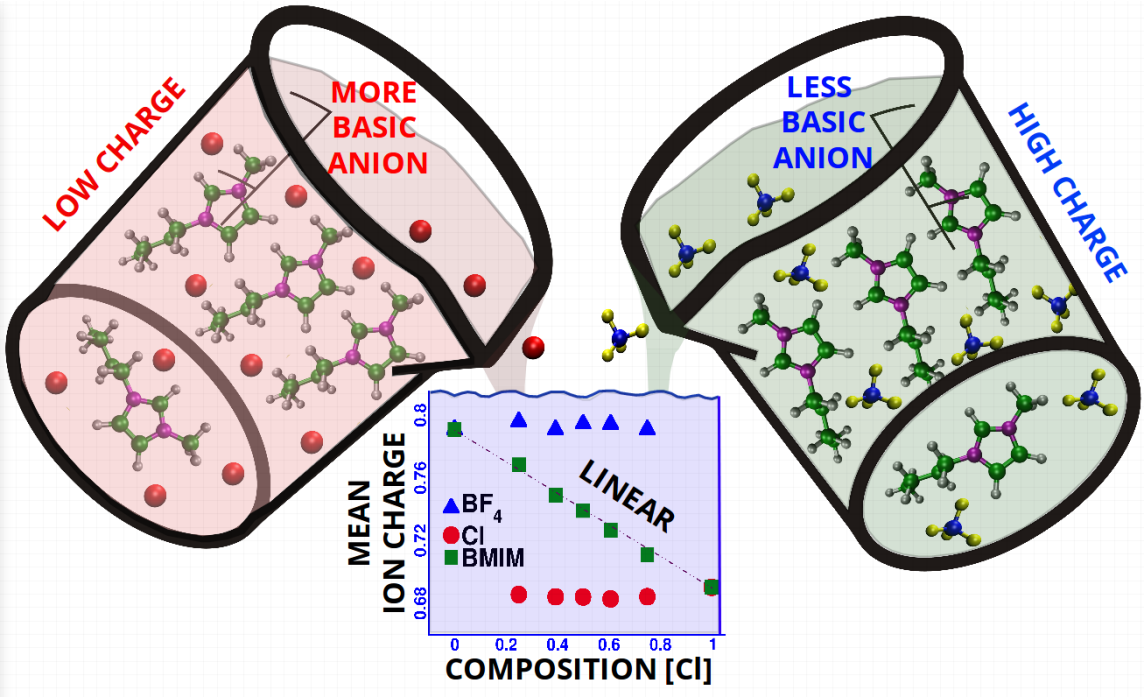

Figure 2A.12: A graphical summary of our work on charge environment in binary ionic liquid mixtures.

Bibliography

[1] Brennecke, J. F.; Maginn, E. J. *AIChE J.* **2001**, *47*, 2384–2389.

[2] Armand, M.; Endres, F.; MacFarlane, D. R.; Ohno, H.; Scrosati, B. *Nat. Mater.* **2009**, *8*, 621–629.

[3] MacFarlane, D. R.; Tachikawa, N.; Forsyth, M.; Pringle, J. M.; Howlett, P. C.; Elliott, G. D.; Davis, J. H.; Watanabe, M.; Simon, P.; Angell, C. A. *Energy Environ. Sci.* **2014**, *7*, 232–250.

[4] Hu, Z.; Margulis, C. J. *P. Natl. Acad. Sci. USA* **2006**, *103*, 831–836.

[5] Bhargava, B. L.; Balasubramanian, S. *J. Chem. Phys.* **2007**, *127*, 114510.

[6] Weingärtner, H. *Angew. Chem. Int. Edit.* **2008**, *47*, 654–670.

[7] Rumble, C. A.; Kaintz, A.; Yadav, S. K.; Conway, B.; Araque, J. C.; Baker, G. A.; Margulis, C.; Maroncelli, M. *J. Phys. Chem. B* **2016**, *120*, 9450–9467.

[8] Zhao, W.; Leroy, F.; Heggen, B.; Zahn, S.; Kirchner, B.; Balasubramanian, S.; Müller-Plathe, F. *J. Am. Chem. Soc.* **2009**, *131*, 15825–15833.

[9] Bedrov, D.; Vatamanu, J.; Hu, Z. *J. Non-cryst. Solids.* **2015**, *407*, 339 – 348.

[10] He, Y.; Qiao, R.; Vatamanu, J.; Borodin, O.; Bedrov, D.; Huang, J.; Sumpter, B. G. *J. Phys. Chem. Lett.* **2016**, *7*, 36–42.

[11] Canongia Lopes, J. N.; Pádua, A. A. *J. Phys. Chem. B* **2006**, *110*, 3330–3335.

[12] Bruce, D. W.; Cabry, C. P.; Lopes, J. N.; Costen, M. L.; D'Andrea, L.; Grillo, I.; Marshall, B. C.; McKendrick, K. G.; Minton, T. K.; Purcell, S. M.; Rogers, S.; Slattery, J. M.; Shimizu, K.; Smoll, E.; Tesa-Serrate, M. A. *J. Phys. Chem. B* **2017**, *121*, 6002–6020.

[13] Morrow, T. I.; Maginn, E. J. *J. Phys. Chem. B* **2002**, *106*, 12807–12813.

[14] Alessandro, B.; Fabio, D.; Giacomo, S. *J. Mol. Liq.* **2007**, *131–132*, 17–23.

[15] Dommert, F.; Schmidt, J.; Qiao, B.; Zhao, Y.; Krekeler, C.; Delle Site, L.; Berger, R.; Holm, C. *J. Chem. Phys.* **2008**, *129*, 224501.

[16] Chaban, V. V.; Prezhdo, O. V. *J. Phys. Chem. B* **2014**, *118*, 13940–13945.

[17] Dommert, F.; Wendler, K.; Berger, R.; Delle Site, L.; Holm, C. *ChemPhysChem* **2012**, *13*, 1625–1637.

[18] Schmidt, J.; Krekeler, C.; Dommert, F.; Zhao, Y.; Berger, R.; Site, L. D.; Holm, C. *J. Phys. Chem. B* **2010**, *114*, 6150–6155.

[19] Son, C. Y.; McDaniel, J. G.; Schmidt, J. R.; Cui, Q.; Yethiraj, A. *J. Phys. Chem. B* **2016**, *120*, 3560–3568.

[20] Uhlig, F.; Zeman, J.; Smiatek, J.; Holm, C. *J. Chem. Theory Comput.* **2018**, *14*, 1471–1486.

[21] Men, S.; Mitchell, D. S.; Lovelock, K. R. J.; Licence, P. *ChemPhysChem* **2015**, *16*, 2211–2218.

[22] Schröder, C. *Phys. Chem. Chem. Phys.* **2012**, *14*, 3089.

[23] Campetella, M.; Gontrani, L.; Bodo, E.; Ceccacci, F.; Marincola, F. C.; Caminiti, R. *J. Chem. Phys.* **2013**, *138*, 184506.

[24] Campetella, M.; Gontrani, L.; Leonelli, F.; Bencivenni, L.; Caminiti, R. *ChemPhysChem* **2015**, *16*, 197–203.

[25] Youngs, T. G. A.; Hardacre, C. *ChemPhysChem* **2008**, *9*, 1548–1558.

[26] Villar-Garcia, I. J.; Lovelock, K. R. J.; Men, S.; Licence, P. *Chem. Sci.* **2014**, *5*, 2573–2579.

[27] (a) [BMIM][Cl] melts at 339K (see the following Ref (b)), thus our simulations of this system are in supercooled liquid state. Despite that, these anions were chosen as (i) they are common and (ii) exhibit the largest total ion charge difference in the respective pure ILs.; (b) Holbrey, J. D.; Reichert, W. M.; Nieuwenhuyzen, M.; Johnson, S.; Seddon, K. R.; Rogers, R. D. *Chem. Commun.* **2003**, 1636–1637.

[28] Clough, M. T.; Crick, C. R.; Grasvik, J.; Hunt, P. A.; Niedermeyer, H.; Welton, T.; Whitaker, O. P. *Chem. Sci.* **2015**, *6*, 1101–1114.

[29] Mondal, A.; Balasubramanian, S. *J. Phys. Chem. B* **2014**, *118*, 3409–3422.

[30] Mondal, A.; Balasubramanian, S. *J. Phys. Chem. B* **2015**, *119*, 11041–11051.

[31] Jorgensen, W. L.; Maxwell, D. S.; Tirado-Rives, J. *J. Am. Chem. Soc.* **1996**, *118*, 11225–11236.

[32] Sambasivarao, S. V.; Acevedo, O. *J. Chem. Theory Comput.* **2009**, *5*, 1038–1050.

[33] Canongia Lopes, J. N.; Deschamps, J.; Pádua, A. A. *J. Phys. Chem. B* **2004**, *108*, 2038–2047.

[34] Lopes, C. J. N.; Deschamps, J.; Pádua, A. A. *J. Phys. Chem. B* **2004**, *108*, 11250–11250.

[35] Canongia Lopes, J. N.; Pádua, A. A. *J. Phys. Chem. B* **2004**, *108*, 16893–16898.

[36] Canongia Lopes, J. N.; Pádua, A. A. *J. Phys. Chem. B* **2006**, *110*, 19586–19592.

[37] Canongia Lopes, J. N.; Pádua, A. A.; Shimizu, K. *J. Phys. Chem. B* **2008**, *112*, 5039–5046.

[38] Plimpton, S. *J. Comput. Phys.* **1995**, *117*, 1–19.

[39] Brown, W. M.; Peng, W.; Plimpton, S. J.; Tharrington, A. N. *Comput. Phys. Commun.* **2011**, *182*, 898–911.

[40] Brown, W. M.; Kohlmeyer, A.; Plimpton, S. J.; Tharrington, A. N. *Comput. Phys. Commun.* **2012**, *183*, 449–459.

[41] Ryckaert, J.-P.; Ciccotti, G.; Berendsen, H. J. C. *J. Comput. Phys.* **1977**, *23*, 327–341.

[42] Nosé, S. *J. Chem. Phys.* **1984**, *81*, 511–519.

[43] Nosé, S. *Mol. Phys.* **1984**, *52*, 255–268.

[44] Martyna, G. J.; Klein, M. L.; Tuckerman, M. *J. Chem. Phys.* **1992**, *97*, 2635–2643.

[45] Perdew, J. P.; Burke, K.; Ernzerhof, M. *Phys. Rev. Lett.* **1996**, *77*, 3865–3868.

[46] Stefan, G. *J. Comput. Chem.* **2006**, *27*, 1787–1799.

[47] Goedecker, S.; Teter, M. *Phys. Rev. B* **1996**, *54*, 1703–1710.

[48] Hutter, J.; Iannuzzi, M.; Schiffmann, F.; VandeVondele, J. *WIREs Comput. Mol. Sci.* **2014**, *4*, 15–25.

[49] Manz, T. A.; Sholl, D. S. *J. Chem. Theory Comput.* **2010**, *6*, 2455–2468.

[50] Manz, T. A.; Sholl, D. S. *J. Chem. Theory Comput.* **2012**, *8*, 2844–2867.

[51] Martinez, L.; Andrade, R.; Birgin, E. G.; Martinez, J. M. *J. Comput. Chem.* **2009**, *30*, 2157–2164.

[52] Hunt, P. A.; Kirchner, B.; Welton, T. *Chem-Eur. J.* **2006**, *12*, 6762–6775.

[53] Kohagen, M.; Brehm, M.; Thar, J.; Zhao, W.; MuÌĹller-Plathe, F.; Kirchner, B. *J. Phys. Chem. B* **2011**, *115*, 693–702.

[54] Sundberg, P.; Larsson, R.; Folkesson, B. *J. Electron. Spectrosc.* **1988**, *46*, 19–29.

[55] Payal, R. S.; Balasubramanian, S. *Phys. Chem. Chem. Phys.* **2013**, *15*, 21077–210833.

[56] Govinda, V.; Attri, P.; Venkatesu, P.; Venkateswarlu, P. *Fluid Phase Equilibr.* **2011**, *304*, 35 – 43.

[57] Matkowska, D.; Hofman, T. *J. Mol. Liq.* **2012**, *165*, 161 – 167.

[58] Almeida, H. F. D.; Canongia Lopes, J. N.; Rebelo, L. P. N.; Coutinho, J. A. P.; Freire, M. G.; Marrucho, I. M. *J. Chem. Eng. Data* **2016**, *61*, 2828–2843.

[59] Bhargava, B. L.; Balasubramanian, S. *J. Phys. Chem. B* **2008**, *112*, 7566–7573.

Chapter 2B

Hydrogen bond dynamics in Binary Ionic Liquid Mixtures

2B.1 Introduction

Hydrogen bonds play a vital role in influencing the bulk properties of ILs, including shear viscosity [1, 2]. Among the many hydrogen bonding sites on the imidazolium cation, the H_A atom (see Figure 2B.1) forms the strongest hydrogen bond with the donor atoms (X) on anions [3, 4]. Hence, for the sake of simplicity, we consider only H_A-X hydrogen bonds. Spectroscopic studies and MD simulations of IL mixtures have shown that H_A-X hydrogen bonds switch from one anion to another as the cation rotates within its solvation shell [5, 6]. Doseok et al. investigated the nature of hydrogen bonds in liquid [BMIM][Cl]$_x$[BF_4]$_{1-x}$ using IR and NMR spectroscopy [6]. While the former showed two *distinct* peaks (C_R-H vibrational modes) corresponding to each type of H_A-X hydrogen bonds, the H_A proton NMR chemical shift showed a single peak whose value exhibited a monotonic change with anion composition. They attributed this conflicting result to the different time scales probed by the two spectroscopic methods – sub-picosecond ($\approx 0.1ps$) for IR and millisecond

Reprinted with permission from "Charge Environment and Hydrogen Bond Dynamics in Binary Ionic Liquid Mixtures: A Computational Study" *J. Phys. Chem. Lett.* **2018**, *9*, 3511–3516. © 2018, American Chemical Society, http://pubs.acs.org/doi/abs/10.1021/acs.jpclett.8b01481.

($\approx 0.6ms$) for NMR. Coalescence of NMR peak when the system's dynamics is faster than coalescence time has been well studied and has been recently extended to vibrational spectroscopy. They conclude that the hydrogen bond switching timescale is higher than the IR time scale and lower than the NMR time scale ($0.1ps < \tau < 0.6ms$). In order to understand these spectroscopic observations, we obtain the timescales of hydrogen bond (HB) switching in pure and mixed ionic liquids.

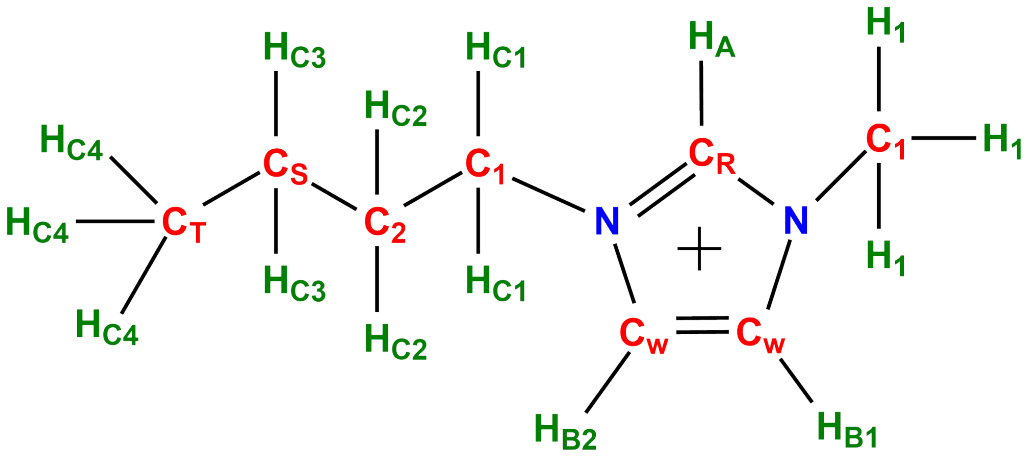

Figure 2B.1: Molecular structure of 1-butyl-3-methylimidazolium cation.

2B.2 Computational Details

Classical molecular dynamics simulations were performed to estimate the hydrogen bond properties in [BMIM][Cl]$_x$[BF$_4$]$_{1-x}$ system. Liquid configurations of 512 ion pairs were created using the PACKMOL package. [7] After an energy minimization in the force field framework, an NPT simulation is run for 10ns at 300K and 1 atm. The last 5 ns of the trajectory was used to determine the equilibrium density. New liquid configurations of 512 ion pairs were created at the equilibrium density. These configurations were equilibrated for 5 ns in NVT ensemble at 300 K. Finally, a production run of 25 ns in NVT followed. The atomic site charges of cation atoms were obtained from linear rule of mixing (described in chapter 2A) and anion atom charges were retained from the corresponding pure systems. All other simulation details are the same as described in chapter 2A.

Hydrogen bond properties were studied by combination of inputs from radial distribution

function (RDF) and time correlation functions (TCF). The estimation of TCFs require the trajectory to be stored at a much higher frequency (typically every femtosecond of simulation time), hence the equilibrium NVT run was extended for another 10ns during which trajectory was stored at higher frequency. The exact values of this frequency (called dump frequency) are mentioned along with the description of each analysis.

2B.2.1 Hydrogen bond definition

In this work, we have incorporated both angle and distance criteria for recognizing a hydrogen bond. Among the many hydrogen bonding sites on the imidazolium cation, the H_A atom (see Figure 2B.1) forms the strongest hydrogen bond with the donor atoms (X) on anions. [3, 4] Although H_B atoms also participate in hydrogen bonding, they are overshadowed by the H_A-X hydrogen bonds, especially at low temperatures. [4] So for simplicity, we consider only H_A-X hydrogen bonds in this study. The H_A-X distance was used for the distance cutoff and $C_R - H_A - X$ angle was used for the angle cutoff. The distance cutoff was taken to be the position of the first minimum of H_A-X pair correlation function and the angle cutoff was taken to be 120^0, as suggested by Hunt *et al*. [4]

2B.3 Results and Discussion

2B.3.1 H_A-X RDF and coordination number

At 50:50 composition, the normalized (by the corresponding value in pure ILs) anion coordination number around H_A (see figure 2B.3) indicates that [Cl] ions are the preferred anions to occupy the first coordination shell of H_A atoms. This is to be expected as [Cl] ions bind stronger to hydrogen bonding sites of cation than [BF_4] ions. However, it should be noted that this preference is only marginal and significant number of [BF_4] ions are also present near the hydrogen bonding sites. This finding is supported by experimental results of IL mixtures as well [5].

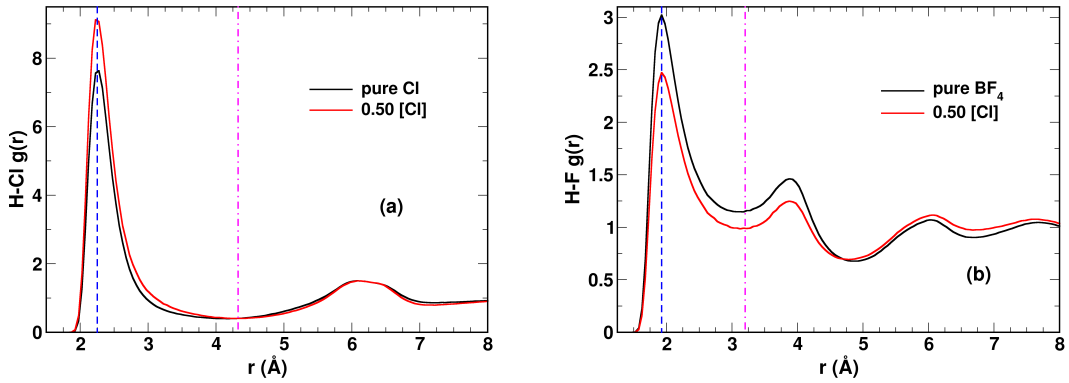

Figure 2B.2: Plots of radial distribution function of (a) H_A with [Cl] ions and (b) H_A with [BF_4] ions (F atom). Blue dashed lines show the position of the first peak and magenta dash-dot lines indicate the position of the first minimum in pure systems.

Table 2B.1: Solvation shell radius and anion coordination number (CN) around H_A.

Anion atom	Composition (x)	r_{min} (Å)	CN	normalized CN
Cl	0.25	4.375	0.4045	0.2968
	0.50	4.325	0.7849	0.5760
	0.75	4.175	1.0931	0.8022
	1.00	4.175	1.3627	1.0000
F	0.00	3.175	2.3824	1.0000
	0.25	3.125	1.6428	0.6896
	0.50	3.125	1.0391	0.4362
	0.75	3.075	0.4682	0.1965
B	0.00	4.875	1.7920	1.0000
	0.25	4.775	1.2724	0.7101
	0.50	4.975	0.8613	0.4806
	0.75	4.725	0.3728	0.2080

2B.3.2 Hydrogen bond population

To estimate the relative propensity of the anions to form hydrogen bonds with cations, we estimate the cation fraction bonded to (i) either one ([Cl] or [BF_4]) of the two anions, (ii) both the anions (called as mixed state) and (iii) no anions. Figure 2B.4 shows these cation fractions as a function of simulation time. It is evident that a majority ($> 90\%$) of cations prefer hydrogen bonding to only one type of anion at a time, [Cl] ions being slightly preferred over the [BF_4] ions. Note that only H_A-X hydrogen bond was considered for this analysis.

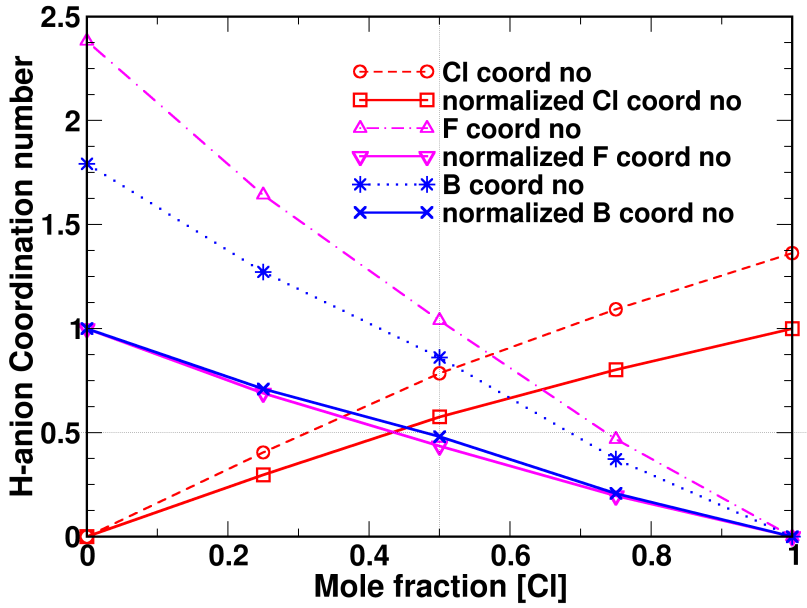

Figure 2B.3: Plot of anion coordination number around H_A atoms with respect to composition.

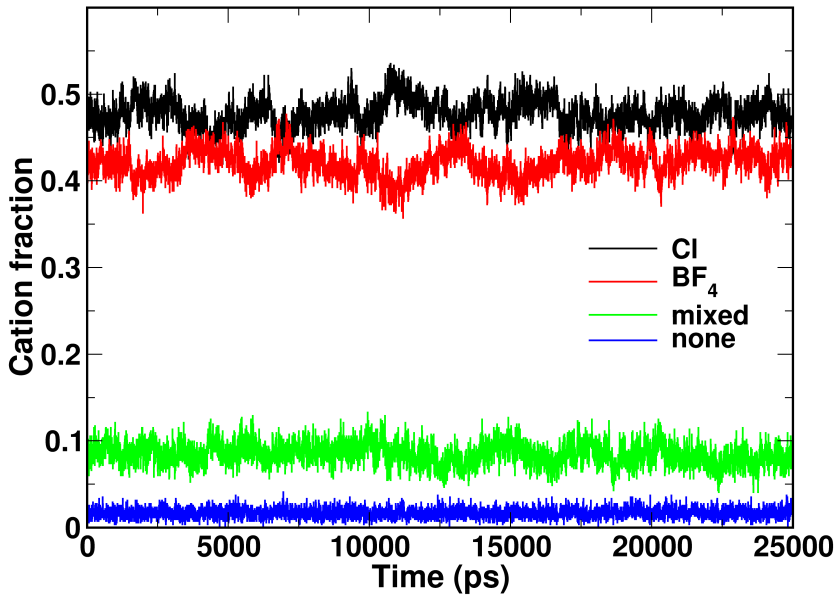

Figure 2B.4: Fraction of cations hydrogen bonded to each of the anions as a function of simulation time. Mixed denotes cations hydrogen bonded to both anion types.

Table 2B.2: Hydrogen bond population.

Cation's hydrogen bond state	percentage
H_A-Cl	47.73%
H_A-F	42.08%
H_A-(Cl and F)	8.50%
No hydrogen bond	1.68%

2B.3.3 Continuous hydrogen bond time correlation functions

The continuous hydrogen bond correlation function (TCF) [8–10] is used to estimate the characteristic time scale of hydrogen bond. It can be defined as –

$$S_{HB}(t) = \frac{\left\langle s_{ab}(t_0)s_{ab}(t+t_0)m_{ab}(t+t_0)\right\rangle}{\left\langle s_{ab}(t_0)^2\right\rangle} \tag{2B.1}$$

where $s_{ab}(t_0)$ is the connectivity matrix between species a and b at time t_0, $m_{ab}(t+t_0)$ is the flag matrix at time $t+t_0$ and $\langle\rangle$ represents the average over time origin t_0. If a and b are connected (in this case hydrogen bonded) at time t, $s_{ab}(t)$ is 1 and is 0 otherwise. The flag matrix $m_{ab}(t+t_0)$ is 0 if the hydrogen bond between a and b is broken at least once between t and t_0; else it is unity. The estimate of $S_{HB}(t)$ from MD trajectory depends on the time between two successive snapshots (dump frequency). Hence we choose the finest dump frequency possible, 1 fs. A trajectory length of 50 ps was analyzed for the 50:50 mixture of [BMIM][Cl]$_x$[BF_4]$_{1-x}$ system. $S_{HB}(t)$ was then fitted to a sum of three exponential decay functions (equation 2B.2) to estimate the hydrogen bond life time.

$$S_{HB}(t) = 1 - \left(\sum_{i=1}^{3} A_i e^{\frac{-t}{\tau_i}}\right) \tag{2B.2}$$

We can classify the hydrogens on the [BMIM] cation into three groups – (i) ring hydrogens (H_A, H_{B1} and H_{B2}) are the most acidic and the strongest hydrogen bond formers, (ii) methylene hydrogens (H_1 and H_{C1}) are the hydrogens attached to carbons which are next to the ring and are barely acidic and do not contribute much to the overall hydrogen

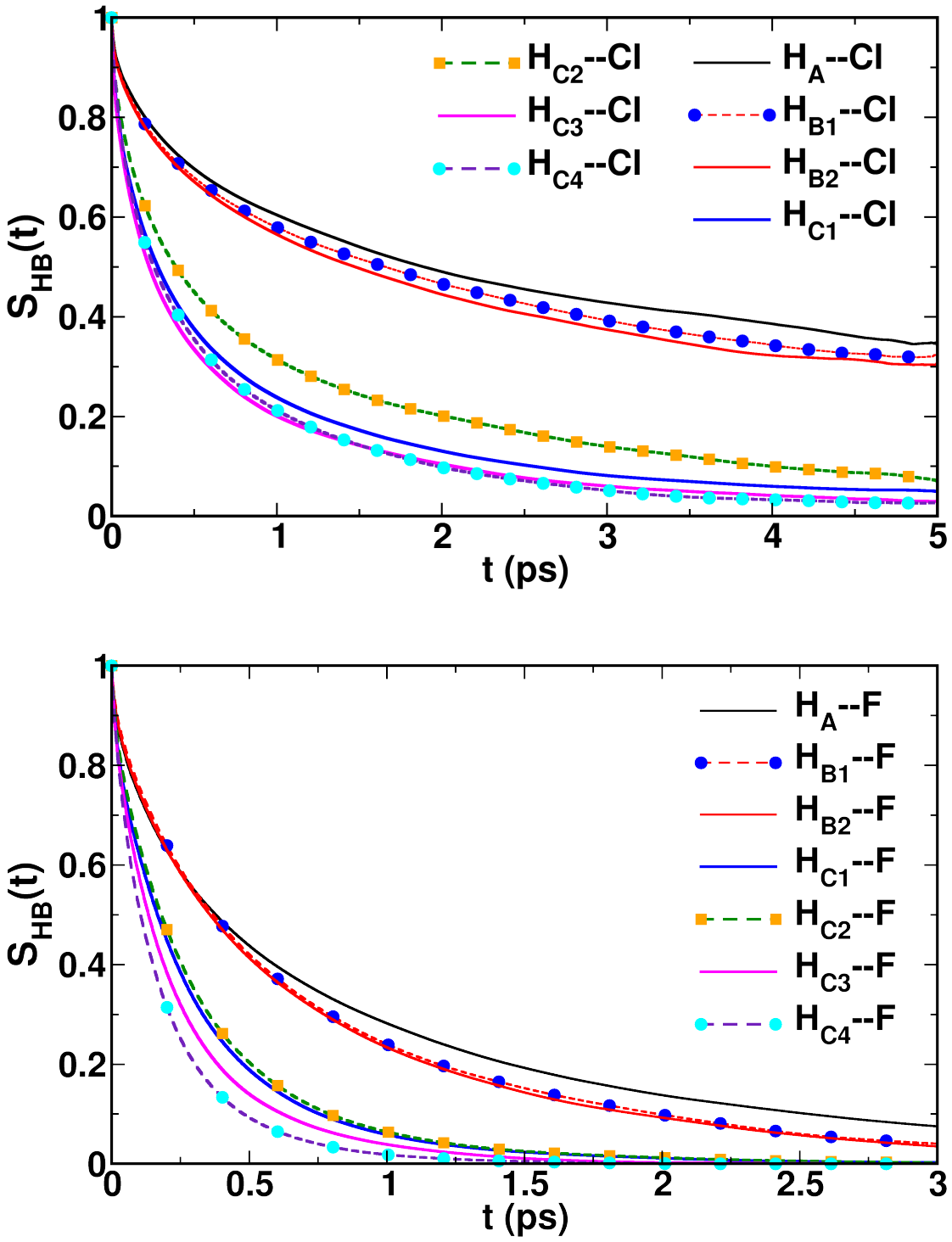

Figure 2B.5: Continuous time correlation function ($S_{HB}(t)$) of hydrogen bond between (a) all hydrogens of the [BMIM] cation and [Cl] ion (H*-Cl), and (b) all hydrogens of the [BMIM] cation and F of [BF_4] anion (H*-F). All the analysis was done for 50:50 mixture of [BMIM][Cl]$_x$[BF_4]$_{1-x}$ system at 300K.

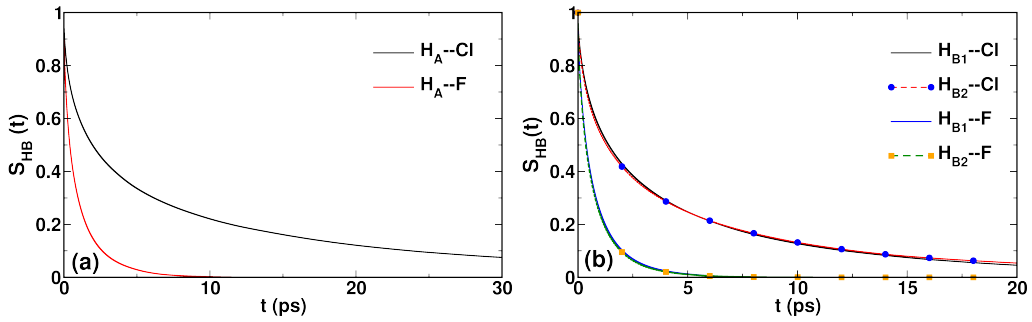

Figure 2B.6: Continuous time correlation function ($S_{HB}(t)$) of hydrogen bond between (a) H_A hydrogens of the [BMIM] cation and [Cl] ion and F atom of [BF_4] ion, and (b) H_B of the [BMIM] cation and and [Cl] ion and F atom of [BF_4] ion. All the analysis was done for 50:50 mixture of [BMIM][Cl]$_x$[BF_4]$_{1-x}$ system at 300K.

bonding network and (iii) tail hydrogens (H_{C2}, H_{C3} and H_{C4}) are connected to the tail part of the cation and cannot form hydrogen bonds. Figure 2B.5 shows that H_A-X bond lasts the longest followed by H_{B1}-X, H_{B2}-X, H_{C2}-X, H_{C1}-X, H_{C3}-X and H_{C4}-X respectively. A clear trend can also be seen with ring hydrogens forming the longest living hydrogen bonds followed by methylene hydrogens and tail hydrogens. Similar trends were reported by Hunt et al. while investigation [BMIM][Cl]. [4] Figure 2B.6 confirms the supposition that [Cl] ion being a stronger hydrogen bond donor than [BF_4] ion results in H*-Cl bond lasting longer than the H*-F bond. Quantitative estimates of the hydrogen bond lifetime values were obtained by fitting the TCFs to exponential decay functions (equation 2B.2). From the lifetime values (table 2B.3), it is evident that H_A-Cl bond lasts longer than the H_A-F bond. This serves as a strong evidence that [Cl] ions are slower in step I than [BF_4] ions (see Section 2B.3.5 for related discussion).

Table 2B.3: Continuous hydrogen bond lifetimes of H_A-X bonds in 50:50 mixture of [BMIM][Cl]$_x$[BF_4]$_{1-x}$ system.

Hydrogen bond	$\langle\tau\rangle$
H_A-Cl	7.7190 ps
H_A-F	0.9605 ps

Table 2B.4: Fit parameters of a sum of three exponential decay functions fitted to the continuous (S_{HB}(t)) time correlation function for the 50:50 mixture.

Hydrogen bond	A_1	τ_1	A_2	τ_2	A_3	τ_3
H_A-Cl	0.2177	0.1486 ps	0.3926	2.1179 ps	0.3898	17.5921 ps
H_A-F	0.1464	0.0305 ps	0.3893	0.3854 ps	0.4643	1.7359 ps

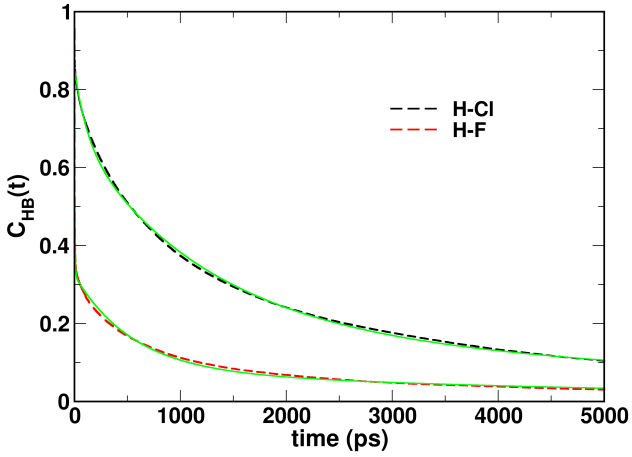

Figure 2B.7: Intermittent hydrogen bond time correlation function plots for [H-Cl] and [H-F] hydrogen bonds in 50:50 BIL mixture. Green continuous lines indicate the fits to the respective TCFs.

2B.3.4 Intermittent hydrogen bond time correlation functions

The intermittent hydrogen bond correlation function (TCF) [8–10] is used to estimate the characteristic time scale of intermittent hydrogen bond (where breaking and reformation of hydrogen bond is allowed). It can be defined as –

$$C_{HB}(t) = \frac{\left\langle s_{ab}(t_0)s_{ab}(t+t_0)\right\rangle}{\left\langle s_{ab}(t_0)^2\right\rangle} \tag{2B.3}$$

where $s_{ab}(t_0)$ is the connectivity matrix between species a and b at time t_0 and $\langle\rangle$ represents the average over time origin t_0. If a and b are connected (in this case hydrogen bonded) s_{ab} is 1 and 0 otherwise. $C_{HB}(t)$ was fitted to a sum of four exponential decay functions. 25 ns of the equilibrium trajectory with a dump frequency of 5 ps was used to

calculate $C_{HB}(t)$ for the 50:50 mixture of [BMIM][Cl]$_x$[BF$_4$]$_{1-x}$ system. Consistent with the $S_{HB}(t)$ results, $C_{HB}(t)$ also shows that H_A-Cl bond lasts longer than H_A-F bond. Table 2B.6 lists the amplitudes and the time constants of the fitted function. C_{HB}(t) also shows similar trends observed via S_{HB}(t), essentially reinforcing the fact that H_A-Cl bond lasts longer than the H_A-F bond which is crucial for further analysis. Again, previous work on [BMIM][Cl] show results inline with our findings. [4]

$$C_{HB}(t) = 1 - \left(\sum_{i=1}^{4} A_i e^{\frac{-t}{\tau_i}} \right) \tag{2B.4}$$

Table 2B.5: Time-constants of intermittent hydrogen bond TCF, in 50:50 mixture, obtained from fitting $C_{HB}(t)$ to four exponential decay functions

Hydrogen bond	$\langle\tau\rangle$
H_A-Cl	2022 ps
H_A-F	1919 ps

Table 2B.6: Fit parameters of a sum of four exponential decay functions fitted to the intermittent ($C_{HB}(t)$) time correlation function for the 50:50 mixture.

Hydrogen bond	A_1	τ_1 (ps)	A_2	τ_2 (ps)	A_3	τ_3 (ps)	A_4	τ_4 (ps)
H_A-Cl	0.15	0.54	0.17	113.9	0.49	1188	0.20	7184
H_A-F	0.38	0.36	0.29	4.81	0.24	545	0.08	5876

2B.3.5 Hydrogen bond switching

In order to understand these spectroscopic observations, we obtain the timescales of hydrogen bond (HB) switching in pure and mixed ionic liquids. We define a time dependent pair correlation function $\tilde{g}_{\mathrm{HX}}(r,t)$ (defined below), between the most acidic hydrogen (H_A) of the cation and the donor atom (X = Cl,F) of the anion.

$$\tilde{g}_{\mathrm{HX}}(r,t) = \frac{V}{\widetilde{N}_{\mathrm{X}} 4\pi r^2} \left\langle \frac{1}{\widetilde{N}_{\mathrm{H}}(t_0)} \sum_{i=1}^{\widetilde{N}_H} \sum_{j=1}^{\widetilde{N}_{\mathrm{X}}} \delta\Big(r - \left| \vec{r}_j^{\,X}(t_0+t) - \vec{r}_i^{\,H}(t_0+t) \right| \Big) \right\rangle \tag{2B.5}$$

$$\tilde{g}_{\mathrm{HX}}(r,t) = \frac{V}{\widetilde{N}_{\mathrm{X}} 4\pi r^2 dr} \left\langle \frac{\tilde{n}_{\mathrm{HX}}(r, t_0 + t)}{\widetilde{N}_{\mathrm{H}}(t_0)} \right\rangle \tag{2B.6}$$

where V is the volume of the simulation box, $\widetilde{N}_{\mathrm{X}}$ is the number of *selected* donor atoms, $\widetilde{N}_H(t_0)$ is the number of $\mathrm{H_A}$ atoms belonging to *selected* cations at time t_0, δ represents the Dirac delta function, $\vec{r}$ represents the position of atoms and $\langle\rangle$ represents the average over time origin t_0. In the case of HB switching between same kind of anion (say [Cl] to [Cl]) $\widetilde{N}_{\mathrm{X}} = N_{\mathrm{X}} - 1$, N_{X} being the total number of X type donor atoms, because the anion hydrogen bonded to cation at time $t = 0$ is not considered in the calculation of $\tilde{g}_{\mathrm{HX}}(r,t)$. Whereas, in the case of HB switching between different anions (say [Cl] to [F]) $\widetilde{N}_{\mathrm{X}} = N_{\mathrm{X}}$. Equation 2B.6 gives a simplified version of $\tilde{g}_{\mathrm{HX}}(r,t)$, where $\tilde{n}_{\mathrm{HX}}(r, t_0 + t)$ is the number of X atoms (in case of like anion switching, we exclude the X atom hydrogen bonded to selected cation at t_0) situated at a distance between r and $r + dr$ from the *selected* $\mathrm{H_A}$ atoms. At time t_0, we select cations which are hydrogen bonded to only one of the two anion types in the mixture. This selected population of cations represents an out of equilibrium scenario where only one type of hydrogen bonding is present. Hence, this population would relax to the equilibrium hydrogen bonding statistics by process of anion exchange. The anion which hydrogen bonds with the cation at any time t can be of the same type as the one that the cation was hydrogen bonded to at time t_0, or it could be of another type. Thus, it is possible to calculate from the MD trajectory at a given composition, four different $\tilde{g}(r,t)$. $\tilde{g}_{\mathrm{HX}}(r,t)$ tells us the time evolution of this anion exchange process (see Figure 2B.8).

In all the $\tilde{g}_{\mathrm{HX}}(r,t)$ plots, we see that the first peak, which is absent at time t_0 increases in intensity with time. This indicates that other anions (i.e., ones which were not initially hydrogen bonded to the selected cations) start replacing the original anions which were hydrogen bonded to the cation initially. To obtain a quantitative estimate of this relaxation process, we compute the radial coordination number $\tilde{c}_{\mathrm{HX}}(t)$. The coordination number is calculated by integrating $\tilde{g}_{\mathrm{HX}}(r,t)$ up to the first solvation shell cutoff. Equation 2B.8 gives a normalized function $f(t)$ which can be used to compare the time scales of different kinds

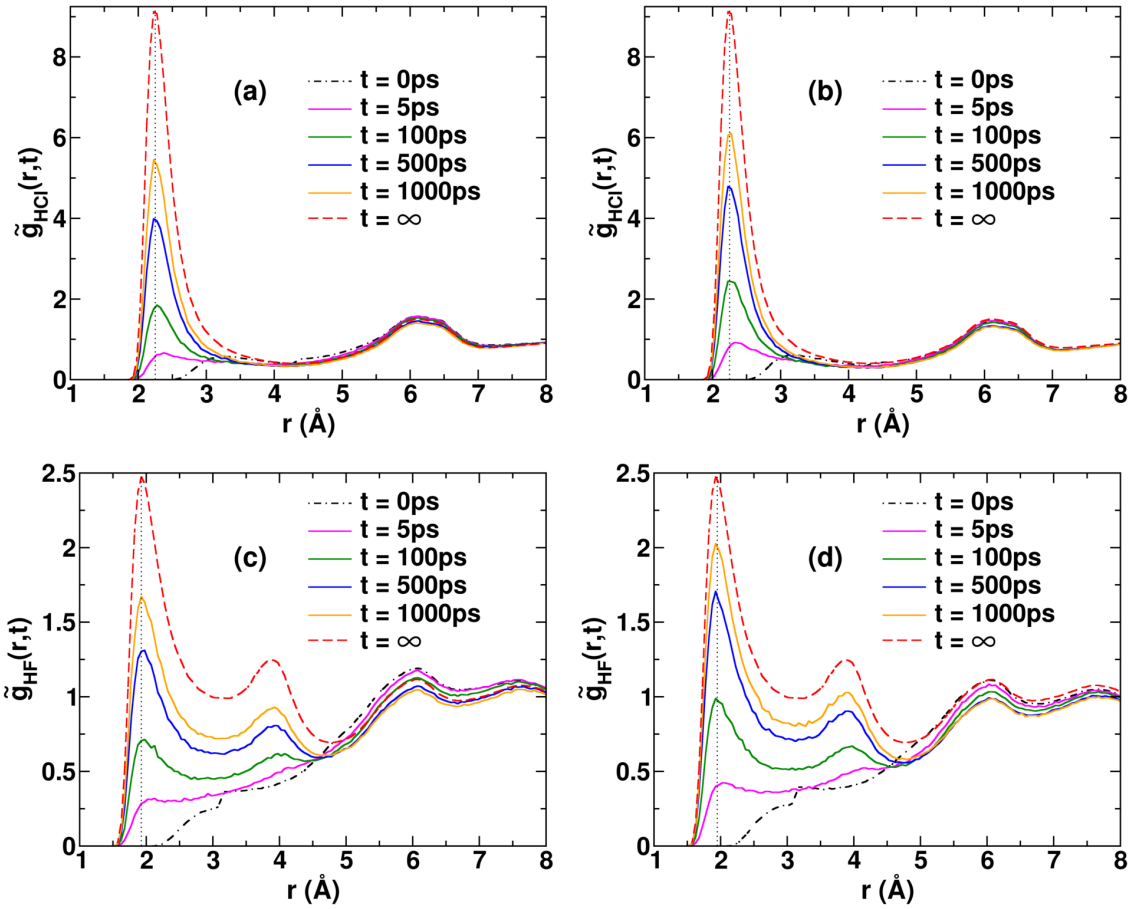

Figure 2B.8: Time evolution of (a) $\tilde{g}_{\mathrm{HCl}}(r,t)$ from the population of cations initially hydrogen bonded to [Cl] ions, (b) $\tilde{g}_{\mathrm{HCl}}(r,t)$ from the population of cations initially hydrogen bonded to [BF_4] ions, (c) $\tilde{g}_{\mathrm{HF}}(r,t)$ from the population of cations initially hydrogen bonded to [Cl] ions and (d) $\tilde{g}_{\mathrm{HF}}(r,t)$ from the population of cations initially hydrogen bonded to [BF_4] ions. 50:50 BIL mixture was used for this analysis. The maroon dotted line indicates the position of the first peak at $t = \infty$ (equilibrium).

of anion exchange.

$$f(t) = \frac{\tilde{c}_{\mathrm{HX}}(t) - \tilde{c}^{0}_{\mathrm{HX}}}{\tilde{c}^{\infty}_{\mathrm{HX}} - \tilde{c}^{0}_{\mathrm{HX}}} \tag{2B.7}$$

where $\tilde{c}^{0}_{\mathrm{HX}}$ is the coordination number at time t_0 and $\tilde{c}^{\infty}_{\mathrm{HX}}$ is the coordination number when the system is in equilibrium ($t = \infty$). Figure 2B.9 shows the function $f(t)$ for all kinds of anion exchange in the 50:50 BIL mixture as well as in the pure ionic liquid systems.

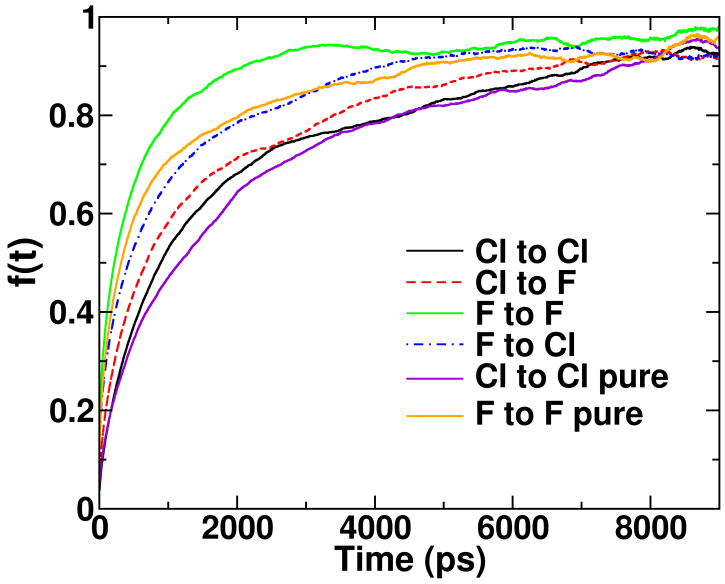

Figure 2B.9: Normalized function $f(t)$ of all kinds of anion exchange in mixed as well as pure ionic liquid systems. Read the labels as: "A to B" to mean coordination number of A type anions with respect to cations that were hydrogen bonded to B type anions at time t_0. The labels with suffix "pure" refers to neat IL systems.

Table 2B.7: Parameters of fit of $f(t)$ to a sum of three exponential functions.

Relaxation process	A_1	τ_1 (ps)	A_2	τ_2 (ps)	A_3	τ_3 (ps)	$\langle\tau\rangle$ (ps)
[Cl] to [Cl]	0.102	13	0.629	975	0.270	7892	2745
[Cl] to [BF_4]	0.102	9	0.472	523	0.426	3984	1919
[BF_4] to [Cl]	0.190	7	0.480	526	0.331	3894	1542
[BF_4] to [BF_4]	0.226	7	0.612	489	0.122	9393	1449

The function $f(t)$ takes a value of 0 at time t=0 and approaches the value of 1 as the subsystem relaxes towards equilibrium. Note that unlike other time correlation functions, $f(t)$ can take values greater than 1, as there is no upper bound from the definition. Production run of 25 ns with 5 ps dump frequency was used to estimate $\tilde{g}_{HX}(r,t)$. We have used multi-exponential decay function to fit $f(t)$. After several iterations, we have found that three exponential decay functions (equation 2B.8) with appropriate bounds on their time constants yielded good (consistent, relevant and good fits) results. Time-constants of the relaxation process, listed in Table 2B.7, were obtained from fitting $f(t)$ to a sum of three

exponential decay functions.

$$f(t) = 1 - \left(\sum_{i=1}^{3} A_i e^{\frac{-t}{\tau_i}} \right) \tag{2B.8}$$

The migration of [Cl] ions to the occupied hydrogen bonding sites are the slowest processes, while the migration of [BF_4] ions to the occupied hydrogen bonding sites are the fastest. We also note that the migration of [Cl] ions to sites occupied by [BF_4] anions (τ =1.9 ns) is *slower* compared to the migration of [BF_4] ions to [Cl] (τ =1.5 ns) occupied hydrogen bonding sites. This might seem counter-intuitive as [Cl] ion forms a stronger hydrogen bond with the cation and hence is more likely to replace [BF_4] ions than vice versa. Such an argument might be valid if the [Cl] ions were freely available in the liquid, ready to displace [BF_4] ions from hydrogen bonded sites. However, [Cl] ions are already hydrogen bonded to other sites (either to a different cation or to other ring hydrogens). Thus we propose a simple, mechanical picture of this anion exchange as a three step process – first, the incoming anion has to break its hydrogen bond and become a free ion (step I), followed by its relative diffusion to the hydrogen bonding location (Step II) and finally, to displace the incumbent anion (Step III). The relative hydrogen bond life time of H_A-Cl, estimated from the continuous hydrogen bond time correlation function is greater than that of H_A-F (see section 2B.3.3). Hence [Cl] ions are slower in step I than the [BF_4] ions. Thus, in the case of [Cl] ions, step I is the rate limiting step and hence they are slow to replace [BF_4] ions than vice versa.

From this study, we estimate the characteristic time scale of the hydrogen bond switching phenomenon to be in the order of nanoseconds (1.4 ns - 2.7 ns). IR spectroscopy, which probes the system at sub-picosecond timescale, essentially captures a static hydrogen bond network and hence detects two distinct C_R-H_A vibrational peaks corresponding to two different H_A-X bond types. But NMR spectroscopy, probing larger time scales, captures a dynamic hydrogen bond network and thus exhibits a single chemical shift value [6].

2B.4 Conclusions

MD simulations performed using the charge mixing rule developed in chapter 2A were used to study hydrogen bonding in binary ionic liquid mixture of [BMIM][Cl]$_x$[BF$_4$]$_{1-x}$ system. H$_\mathrm{A}$-X pair correlation functions reveal the relative propensity of [Cl] and [BF$_4$] ions towards the most acidic hydrogen H$_\mathrm{A}$. Though [Cl] ions occupy the first solvation shell of H$_\mathrm{A}$ preferentially over [BF$_4$] ions, this preference is marginal with significant number of [BF$_4$] ions also present in the first solvation shell. The real difference between the hydrogen bonding ability of [Cl] and [BF$_4$] ions was revealed by the order of magnitude difference in the continuous hydrogen bond lifetimes with H$_\mathrm{A}$-Cl bond lasting much longer than H$_\mathrm{A}$-F bond. These lifetimes also revealed that the ring hydrogens are the strongest hydrogen bond formers followed by the methylene and tail hydrogens, consistent with previous findings. [4]

To estimate the timescale of exchange of anions between the H$_\mathrm{A}$-X hydrogen bonding sites, we have devised a time dependent pair correlation function $\tilde{g}_{\mathrm{HX}}(r,t)$. $\tilde{g}_{\mathrm{HX}}(r,t)$ is defined in such a way that appearance of first peak indicates that X atoms are replacing the incumbent hydrogen bond acceptors. To get quantitative estimates of the hydrogen bond switching process, we have defined a function $f(t)$ based on the time dependent coordination number $\tilde{c}_{\mathrm{HX}}(t)$.

The hydrogen bond switching is shown to be a three step process involving hydrogen bond breaking, relative diffusion and hydrogen bond forming respectively. The timescales of each of these processes have been determined which rationalize the differences in experimental results of IR and NMR spectroscopies.

Bibliography

[1] Hunt, P. A. *J. Phys. Chem. B* **2007**, *111*, 4844–4853.

[2] Gehrke, S.; von Domaros, M.; Clark, R.; Holloczki, O.; Brehm, M.; Welton, T.; Luzar, A.; Kirchner, B. *Faraday Discuss.* **2018**, *206*, 219–245.

[3] Thar, J.; Brehmy, M.; Seitsonen, A. P.; Kirchner, B. *J. Phys. Chem. B* **2009**, *113*, 15129–15132.

[4] Skarmoutsos, I.; Welton, T.; Hunt, P. A. *Phys. Chem. Chem. Phys.* **2014**, *16*, 3675–3685.

[5] Matthews, R. P.; Villar-Garcia, I. J.; Weber, C. C.; Griffith, J.; Cameron, F.; Hallett, J. P.; Hunt, P. A.; Welton, T. *Phys. Chem. Chem. Phys.* **2016**, *18*, 8608–8624.

[6] Cha, S.; Kim, D. *Phys. Chem. Chem. Phys.* **2015**, *17*, 29786–29792.

[7] Martinez, L.; Andrade, R.; Birgin, E. G.; Martinez, J. M. *J. Comput. Chem.* **2009**, *30*, 2157–2164.

[8] Rapaport, D. C. *Mol. Phys.* **1983**, *50*, 1151–1162.

[9] Chandra, A. *Phys. Rev. Lett.* **2000**, *85*, 768–771.

[10] Balasubramanian, S.; Pal, S.; Bagchi, B. *Phys. Rev. Lett.* **2002**, *89*, 9–12.

Chapter 3

Development and validation of a force field model for Oligomeric Ionic Liquids

3.1 Introduction

Ionic liquids are often touted as "designer solvents" because of the possibility of designing a solvent of choice by choosing appropriate cations and anions. [1] In an attempt to expand the choice of ions, Armstrong *et al.* devised a new strategy to synthesize cations. They prepared thirty-nine geminal dicationic ionic liquids (DILs) which showed better thermal stabilities compared to the monomeric ionic liquids present at that time. [2] They also noted that many of these dicationic ionic liquids are solids at room temperature. They noticed an increase in density and viscosity (>240 cSt) with increase in chain length. [3] Due to their superior stability, volatility, DILs have been used in gas chromatograpy, as high temperature lubricants, in catalysis *etc.* [4–7]

Lee *et al.* investigated a series of ether functionalized cations to study the effects of functionalization on the viscosity. [8] They conclude that ether functionalization indeed results in reduced viscosity and propose this functionalization as a strategy to reduce the viscosity of ionic liquids. Teng *et al.* investigated the use of ether linked DILs and their mixtures with monomeric ILs for their use in electric double layer capacitors and found improved performance in case of DILs. [9]

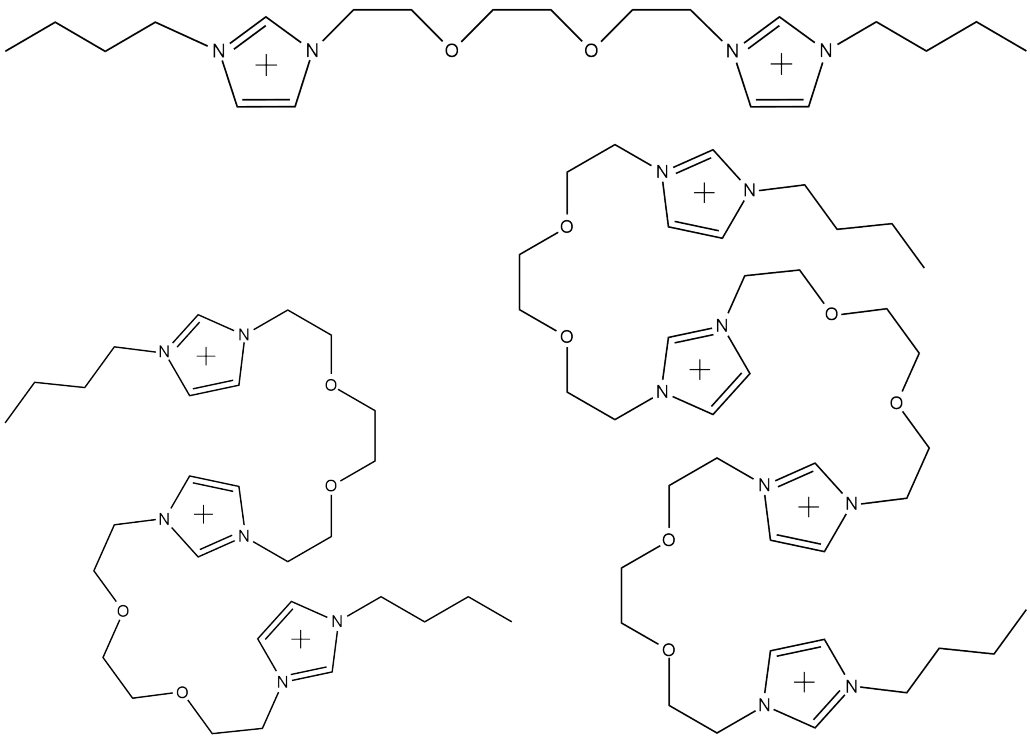

Figure 3.1: Chemical structure of (a) IL2, (b) IL3, (c) IL4 cations

Extending the concept of DILs, Aida *et al.* designed a new class of ionic liquids called oligomeric ionic liquids (OILs). [10] These are Ionic liquids containing imidazolium based monomeric units linked together via ether linkages. Figure 3.1 shows the chemical structure of IL2, IL3 and IL4 cations with two, three and four imidazolium rings respectively connected via ether linkages. These OILs showed unprecedented performance in graphene exfoliation with 93% yield and 95% purity in under 30 minutes. Aida *et al.* then investigated the same class of OILs for their use in electrochemical devices. [IL4][NTf_2] showed the best EDL performance (with EDL capacitance of 64 $\mu F/cm^2$) of an ionic liquid which is about 6 times higher than that of monomeric ionic liquid [BMIM][NTf_2].

Recently Wu *et al.* investigated oligomeric ionic liquids (OILs) using classical density functional theory (CDFT). [11] They conclude that oligomeric cations have little improvement to the charging behaviour on the positive electrode while they enhance the energy storage density at the negative electrode. This is to be expected as the structure of electric double layer (EDL) at the positive electrode would be rich in anions and that of negative electrode would be rich in cations. Though CDFT calculations give some insight into the

capacitive behaviour of OILs at interfaces, this model is too coarse grained to consider the details of the linkers. Aida *et al.* noted that the choice of linkers can have drastic effects the properties of the system. [12] Though OILs have such exceptional properties, molecular level insights are lacking which makes the tuning the properties of these liquids a difficult task. For example, viscosity of these OILs are still too high to find practical applications in electrochemical devices. [12]

This chapter presents the work done towards modelling this emerging class of oligomeric ionic liquids using quantum chemical and molecular dynamics simulations. The next section elucidates the methodology used for this study followed by results and discussion then ending with conclusions.

3.2 Methodology and Computational details

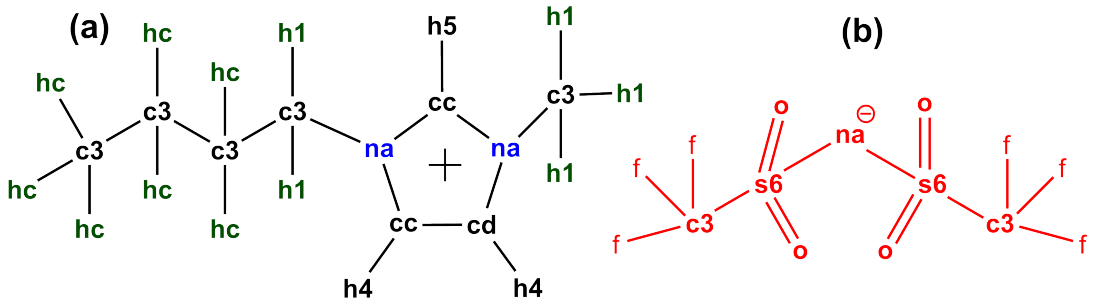

Figure 3.2: Chemical structures labelled with GAFFF atom types of (a) [BMIM] cation, (b) [NTf_2] anion.

3.2.1 Force field

Though there exists many refined force fields for imidazolium based ionic liquids, they are unsuitable for modelling OILs because of the lack of transferability (For instance though CL&P force field has parameters for imidazolium cation, it does not have parameters for the ether linkage of OILs). [13–21] A general force field with suitable modifications should serve as a good starting point for modelling OILs. [22–24] The general AMBER force field (GAFF) was shown to accurately predict thermodynamic and transport properties of many ionic liquids, including the ones based on imidazolium cations. [25] Moreover, Maginn *et*

al. have refined the GAFF force field for ethers by scaling the van der Waals parameters thereby retaining its transferability. [26] In this work, we use the GAFF force field for the [NTf_2], imidazolium and the tail parts and Maginn's modified parameters for the linker part of the OILs.

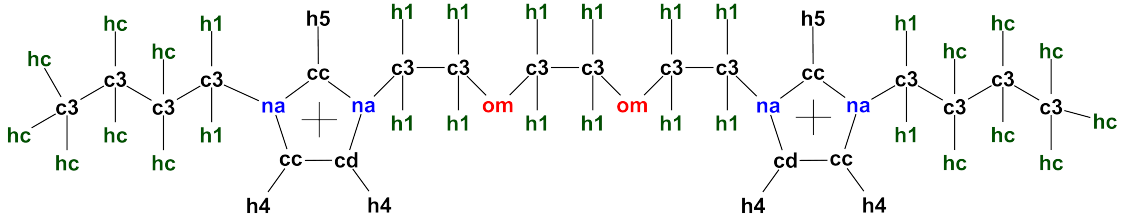

Figure 3.3: Chemical structure of IL2 cation along with GAFF atom types used in this study.

3.2.2 Atomic Site Charges

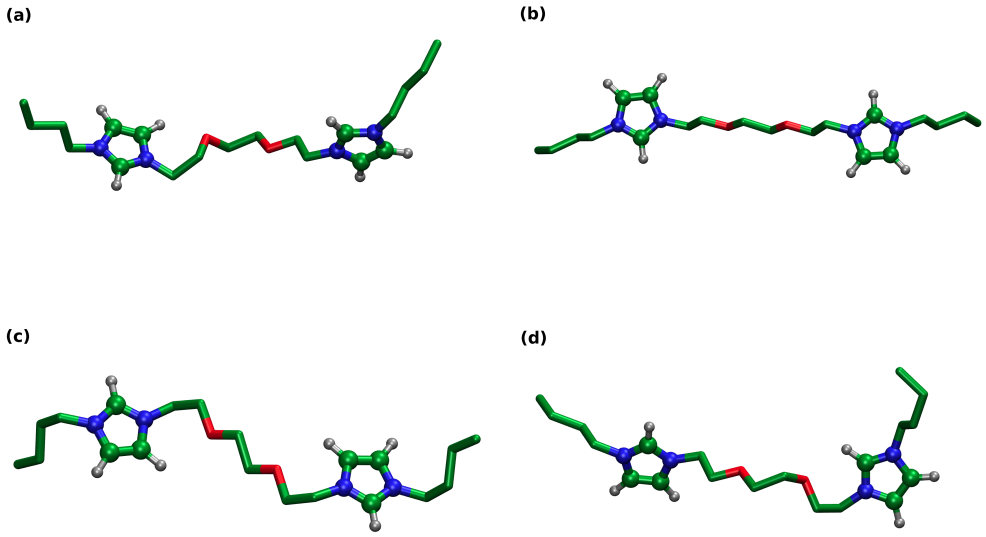

Figure 3.4: Configurations of IL2 ion obtained by geometry optimizing hand built structures (a-b) and geometry optimizing arbitrarily chosen snapshots obtained from gas phase MD simulation (c-d). IL2 atom color index – Silver : H, Green : C, Blue : N, Red : O.

As described in chapter 1.0.6, atomic site charges are crucial for a force field to accurately reproduce experimental data. Hence care was taken to refine atomic site charges for use with GAFF force field. GAFF force field prescribes the use of restrained electrostatic

potential (RESP) method at HF/6-31G* level to obtain atomic site charges. [22, 27, 28] In the context of molecular dynamics (MD) simulations, DDEC charges show superior characteristics when compared to RESP charges. [19, 20, 29, 30] However, using DDEC charges would require, at the least, reparametrization of van der Waals and dihedral parameters, which in the absence of sufficient experimental data would be a futile effort.

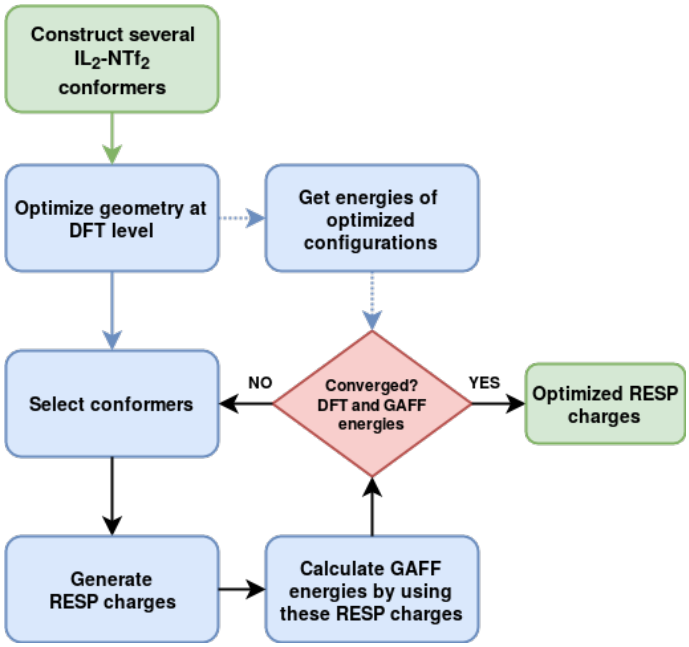

Figure 3.5: Flowchart of the process used to refine atomic site charges.

To obtain the RESP charges, several gas phase configurations of ion pairs containing one IL2 and two NTF_2 molecules were created. Though the gas configurations of ion pairs do not resemble the liquid phase environment, charges obtained from them can serve as a good starting point. [31] First, three configurations of IL2 were built by hand using Gaussview software. [32] A subsequent gas phase MD run was carried out with one IL2 ion to sample three more configurations at random from the trajectory. Figure 3.4 shows snapshots of two representative IL2 ion configurations. This random sampling allows for selecting configurations that might be otherwise inaccessible to human intuition. Each of these configurations were then geometry optimized at B3LYP/6-31G(d,p) level using Gaussian 09 software. [33] Ten ion pair configurations were then constructed by placing two NTF_2 ions around previously optimized IL2 ions and then geometry optimized at

B3LYP/6-31G(d,p) level. RESP charges were generated for each configuration using RED-tools. [34] Different charge sets can be obtained by fitting the electrostatic potential of each of the optimized configurations individually or by selecting any combination of configurations to be fit simultaneously. To choose an optimal charge set, we used an iterative refinement procedure, as described in Figure 3.5. For each charge set generated, GAFF energies of the ten gas phase [IL2][NTf_2] configurations are compared against the corresponding DFT B3LYP/6-31G(d,p) energies. The root mean squared error (RMSE) of the energies between GAFF and DFT was used as the penalty score. RESP charges obtained from several different combinations of configurations were tried until a satisfactory agreement (low penalty score) between DFT and GAFF energies was seen. Incidentally, the optimized charges obtained in this manner are the RESP charges obtained from the most stable configuration. In other words, RESP charges of the most stable configuration shows the best agreement between DFT and GAFF energies. Table 3.2 lists the Lennard-Jones parameters of the atom types used in this study (See Appendix for a list of optimized atomic site charges).

Table 3.1: Classical MD simulation box details for [IL2][NTf_2] and [BMIM][NTf_2] systems.

System	Number of Cations	Number of Anions	Box Size (Å)
IL2 NTf_2 (bulk)	256	512	64.82
BMIM NTf_2 (bulk)	512	512	62.60

3.2.3 MD simulations

All atom molecular dynamics (MD) simulations were carried out to simulate bulk liquid and liquid-vapor interface of [IL2][NTf_2] using the GAFF force field and our refined charges. First, a isothermal-isobaric (NPT) simulation was carried out at 300K and 1 atm to obtain the equilibrium density. The simulation was run for 45ns out of which the last 10ns data was used to estimate equilibrium density. A subsequent isothermal (NVT) run was carried out at 300 K at the equilibrium box size. Due to the sluggish behaviour of the [IL2][NTf_2] system (see section 3.3), five independent runs were used for all analyses. The

Table 3.2: Lennard-Jones parameters of the modified GAFF force field used in this study.

Atom	ϵ (KJ mol^{-1})	σ (Å)
cc	0.08600	3.3996695
h4	0.01500	2.5105526
cd	0.08600	3.3996695
na	0.17000	3.2499985
h5	0.01500	2.4214627
c3	0.10940	3.3996695
h1	0.01570	2.4713530
hc	0.01570	2.6495328
os	0.17000	3.0000123
cm	0.09846	3.5016596
om	0.15300	3.0900127
hm	0.01413	2.5454936
c3	0.10940	3.3996695
s6	0.25000	3.5635949
ne	0.17000	3.2499985
sy	0.25000	3.5635949
o	0.21000	2.9599219
f	0.06100	3.1181455

initial configuration for each independent run was generated by a charge scaling procedure outlined in Figure 3.6. Table 3.1 lists the simulation box details the bulk liquid and liquid-vapor interface simulations. The Nosé-Hoover thermostat with a damping parameter of 0.1 ps and barostat with a damping parameter of 1 ps were used to generate positions and velocities from NPT and NVT ensembles. [35–37] Velocity Verlet integrator with 1 fs time step was used to solve the equations of motion. All C-H bonds were constrained using SHAKE algorithm as implemented in LAMMPS. [38] A cut-off of 12 Å was used for non-bonded interactions and long range electrostatic interactions were solved with an accuracy of 10^{-5} using the particle-particle particle-mesh (PPPM) solver. Tail corrections were applied for the calculation of energy and pressure. All MD simulations were carried out using LAMMPS package. [39–41] Initial liquid configurations of all systems were created using PACKMOL package. [42]

Surface tension was estimated from the liquid-vapor interface simulations. The liquid-vapor interface was created by extending the z dimension of the pre-equilibrated NVT box to 300 Å. An NVT simulation was carried out for 20 ns and the last 4 ns trajectory was

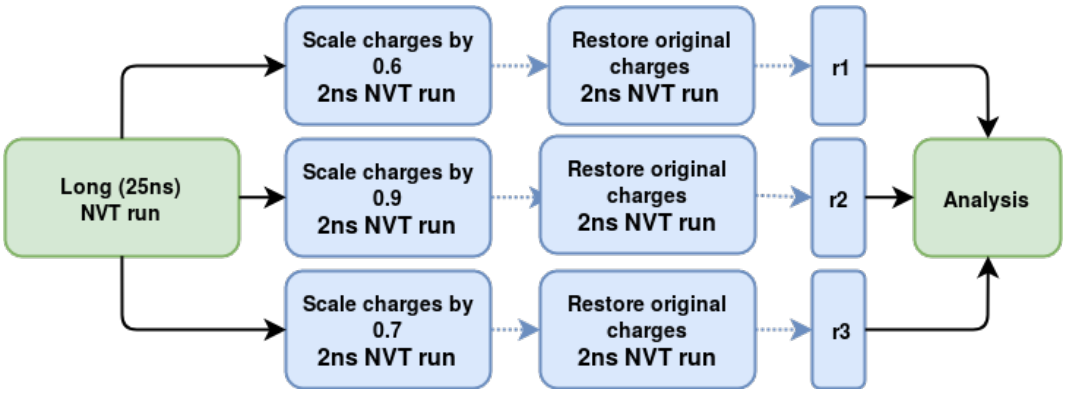

Figure 3.6: Charge scaling procedure to generate multiple independent trajectories.

used for analysis. The pressure tensor was written to a file every timestep and the surface tension was calculated using equation 3.1. l_z is the box dimension in the z-direction, P_{xx}, P_{yy} and P_{zz} are the normal components of the pressure tensor in the x, y and z directions respectively.

$$\gamma = \frac{l_z}{4}(2P_{zz} - P_{xx} - P_{yy}) \tag{3.1}$$

A peculiar case of negative surface tension was observed throughout the 20ns trajectory as seen in Figure 3.7. We speculated that the system was stuck near an abnormal configuration (as the simulation was started with bulk like configuration) and the sluggish nature of the liquid did not allow the system to equilibrate in the given time of 20 ns. So, we used the charge scaling approach as described in figure 3.6 to generate five independent configurations. Each independent configuration was later run for 24 ns each and the last 12 ns was used for analyses.

[BMIM][NTf_2] system was also simulated with GAFF force field to compare it with [IL2][NTf_2] system. BMIM-NTF_2 ion pair configuration was geometry optimized at MP2 level using correlation consistent aug-cc-pVDZ basis set as implemented in Gaussian 09. [33] The optimized geometry was then used to derive RESP charges using RED-tools. [34] All the parameters used for bulk liquid MD simulations are the same as that of [IL2][NTf_2] system. As the [BMIM][NTf_2] system is not as sluggish as [IL2][NTf_2]

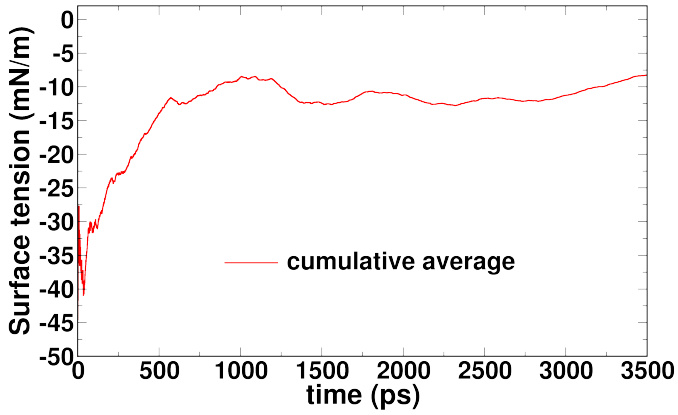

Figure 3.7: Cumulative average of the instantaneous surface tension of [IL2][NTf_2] system at 300K calculated from the last 4 ns of 20 ns trajectory.

system, multiple independent trajectories were not used.

3.3 Results and Discussion

3.3.1 Density

Table 3.3 lists the estimated densities of [IL2][NTf_2] and [BMIM][NTf_2] systems using GAFF force field and their corresponding experimental densities. A maximum deviation of 3% with respect to experiments is observed. Pfaendtner *et al.* also estimated the density of [BMIM][NTf_2] system using GAFF force field and an ad hoc scaling factor of 0.8 to scale all atomic site charges. [25] They report a density of 1.416 g/cc which is again within 1.3% of experimental density. The popular CL&P force field estimates the density of [BMIM][NTf_2] system to be 1.48 g/cc which is very close to our estimated density. [16] In sum, GAFF force field with our refined parameters closely reproduces the density of simulated systems.

Table 3.3: Estimated densities for [IL2][NTf_2] and [BMIM][NTf_2] systems.

System	ρ_{sim}	ρ_{exp}	$\Delta\rho(\%)$
IL2 NTf_2	1.443	1.4	+3.05%
BMIM NTf_2	1.454	1.437	+1.18%

3.3.2 Surface Tension

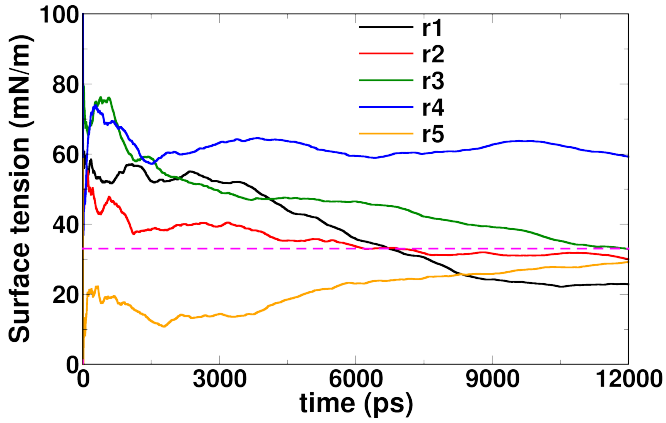

Figure 3.8: Cumulative average of the instantaneous surface tension of [IL2][NTf_2] system for each of the five independent runs. Experimental surface tension is shown with a pink dashed line.

Figure 3.8 shows the cumulative average of instantaneous surface tension for each of the five independent runs. All the runs seem to have converged to their corresponding apparent surface tension values. The average and standard deviation from the five runs came out to be 34 mN/m and 14 mN/m respectively which is very close to the experimental value of 33 mN/m showing only a 3% deviation.

3.3.3 Local Structure

Figure 3.9 shows the radial distribution function between cation rings for [BMIM][NTf_2] and [IL2][NTf_2]. For the IL2 system, RDF between all ring pairs(including intramolecular ring) were considered to generate the red plot and only intermolecular ring pairs were considered for the blue plot. Both BMIM and IL2 systems show a shoulder at 5 Å, with the BMIM system showing a greater intensity than the IL2 one. This prepeak is seen in other imidazolium based ionic liquids as well and is attributed to local stacking of cation rings. [43, 44] The prepeak of intermolecular ring-ring RDF is smaller than the total ring-ring RDF implying that both intra and intermolecular pairs contribute to the peak. Intramolecular ring-ring distance probability density function reveals a broad unimodal peak at 8 Å, implying that the linker does not encourage the intramolecular rings to form

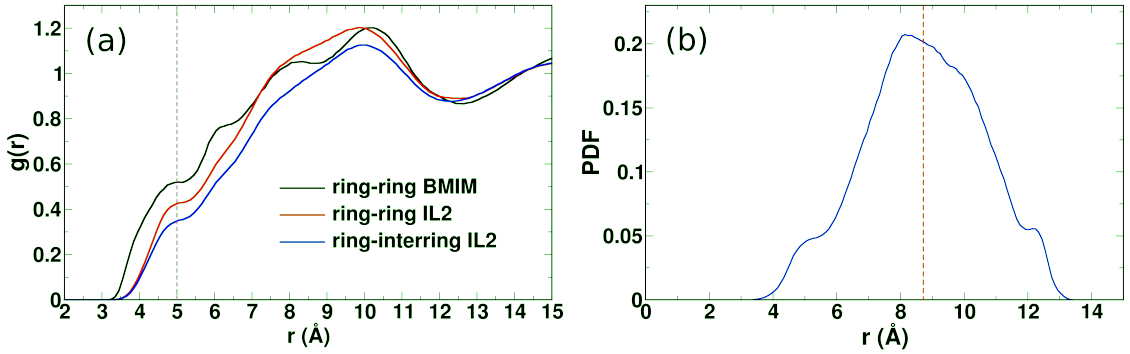

Figure 3.9: (a) Radial distribution function between cation ring centers. Black: inter-ring RDF in [BMIM][NTf_2] system, Red: ring-ring RDF (including intramolecular rings) in [IL2][NTf_2] system, Blue: intermolecular ring-ring RDF in [IL2][NTf_2] system. (b) Probability density function of intramolecular ring-ring distance in the [IL2][NTf_2] system. The red dashed vertical line represents the mean distance of the two rings of the IL2 ion.

a stack. The arrangement of anion atoms from the ring centers for IL2 system seems to be similar to that of BMIM system as shown in Figure 3.10. The RDFs between most acidic hydrogen H_a of the cation and hydrogen bond acceptor atoms of the anion also show similar peaks for IL2 and BMIM system. Oxygen atoms of NTF_2 have the highest first peak followed by nitrogen and fluorine atoms successively for both IL2 and BMIM systems. Similar results were reported for geminal dicationic ionic liquids, where two imidazolium rings are connected via an alkyl linker. [45]

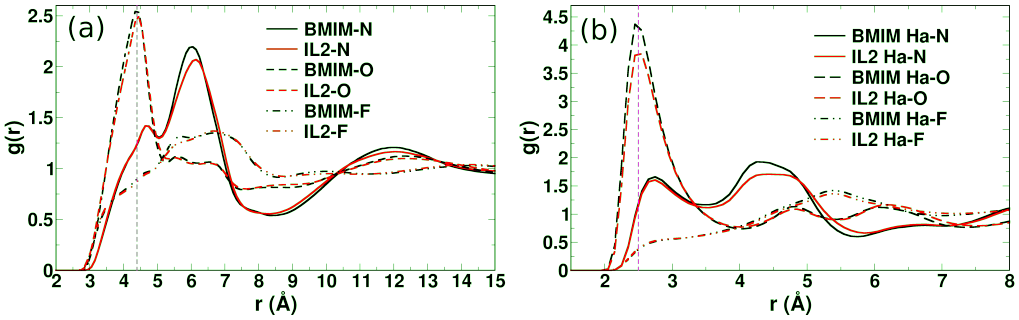

Figure 3.10: Radial distribution functions between (a) cation ring centers and anion atoms for both [BMIM][NTf_2] and [IL2][NTf_2] systems, (b)cation H_a atoms and anion atoms (X) for both [BMIM][NTf_2] and [IL2][NTf_2] systems. All the plots for [BMIM][NTf_2] system are shown in black and [IL2][NTf_2] system are shown in red.

Ordering around oxygen atoms of the linkers (O_m) was also investigated to understand

the influence of ether linkage on the overall ordering in the IL2 system. RDF between O_m and H_a atoms shows two strong peaks at 2.65 Å and 4.9 Å. To delineate the contributions of intra and intermolecular H_a atoms to these peaks, RDF between O_m and intermolecular H_a atoms is also shown in Figure 3.11. It's clearly evident that the first two peaks are of intramolecular origin, further supported by O_m-H_a probability density function plot.

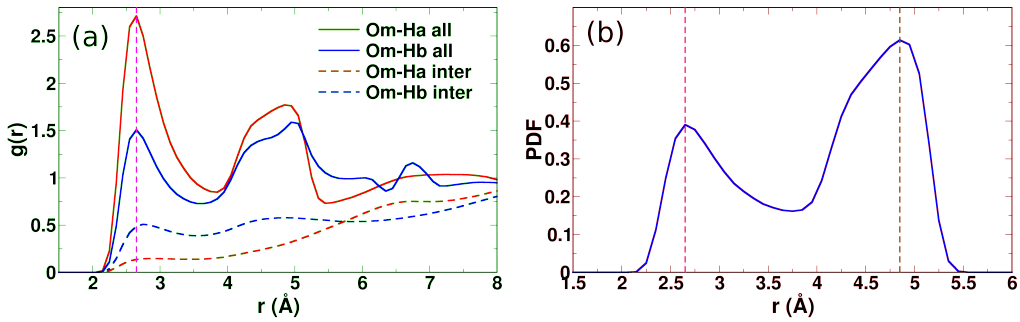

Figure 3.11: (a) Radial distribution functions between cation linker's O_m atoms and (H_a, H_b atoms), (b) probability density function of the distance between intramolecular O_m and H_a atoms. The magenta and green dashed vertical lines indicate the peak positions at 2.65 Åand 4.9 Årespectively.

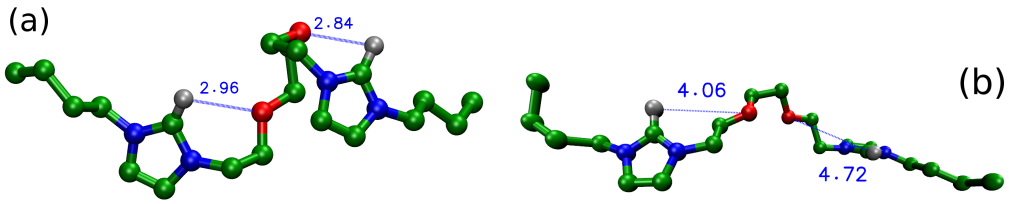

Figure 3.12: Representative configurations of IL2 ion in (a) bound state i.e., H_a atoms are hydrogen bonded to O_m atoms of the same ion and (b) free state i.e., H_a atoms are *not* hydrogen bonded to O_m atoms of the same ion. These configurations were identified in the NVT run of liquid [IL2][NTf_2] system.

The bimodal nature of the O_m-H_a PDF reveals that H_a atoms can be either an intramolecular bound state or an free state as exemplified by the snapshots in Figure 3.12. A H_a atom is considered to be in a intramolecular bound state when the distance between H_a and O_m atoms is less than 3.85 Å(taken to be the first minimum from PDF). 36 % of all H_a atoms are found to be in bound state and 64 % in the free state. To look at the influence that H_a atoms being in bound state has on the ordering around H_a atoms, RDFs of H_a-X (X=atoms

of NTF_2) were separately calculated for bound and free states. Figure 3.11 shows that the bound H_a atoms have shorter first peak the free ones, while the free H_a atoms have the same peak height as that of H_a atoms in the [BMIM][NTF_2] system. Aida *et al.* reported that OILs with alkylene linkers instead of ether linkers have much higher viscosity (to the point of being called solids), but did not investigate the microscopic origin of this disparity. [12] The fact that the intramolecular O_m-H_a hydrogen bonding hinders the H_a-X hydrogen bonding might be disrupting the cation-anion hydrogen bond network and resulting in a reduction in viscosity. But further studies of linker conformations and their effect on the system's ordering are required to conclusively prove this point.

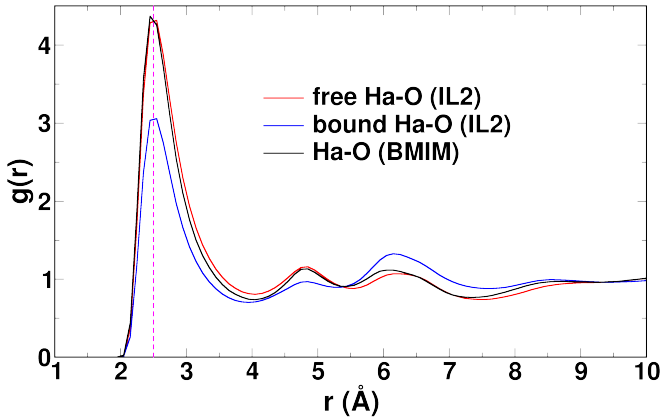

Figure 3.13: Radial distribution functions between cation's H_a atoms and anion's O atoms. Black plot represents the RDF for BMIM system, the red plot represents the RDF between free H_a and O atoms, the blue plot represents the RDF between free bound H_a and O atoms

3.3.4 Interfacial Structure

The surface tension of IL2 and BMIM systems are very close, 33mN/m and 33.09 mN/m respectively. [10, 46] Similar observation was made for the case of dicationic ionic liquids, where the attachment of an alkyl linker between two imidazolium rings hardly changed the surface tension when compared to that of monomeric IL. [2, 3] Figure 3.14 shows the angle distribution of the alkyl tails of the interfacial cations with respect to the positive z axis. IL2 ions within 5 Å of the liquid-vacuum interface are considered to be interfacial cations. A clear orientational ordering is seen, similar to that observed in other

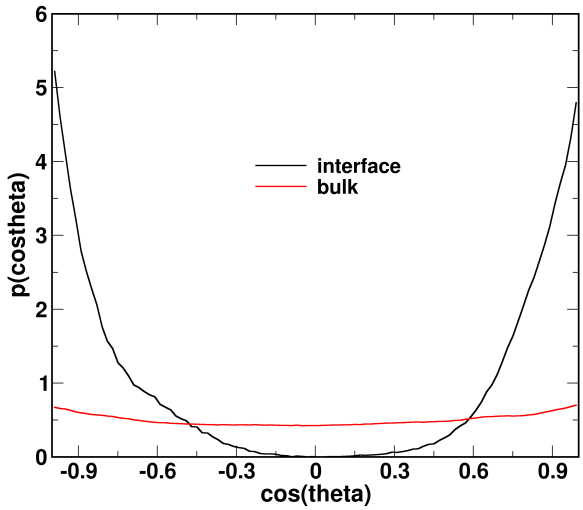

Figure 3.14: Probability density function of the angle made by alkyl tails of the cations w.r.t surface normal (taken to be +z vector) at the liquid-vapor interface of the IL2 system at 300K.

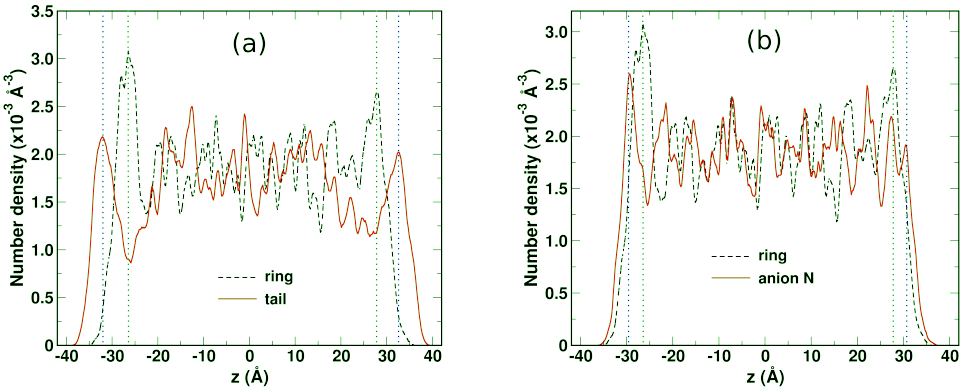

Figure 3.15: (a) Number density profile of cation ring centers and cation tail terminal carbons as a function of z coordinate and (b) number density profile of cation ring centers and anions' N atoms as a function of z coordinate.

monomeric ionic liquids at the liquid-vacuum interface. [47] The number density profile of alkyl tails and cation rings also confirms that the alkyl tails point out into the vacuum part of the interface. A slight preference of anions when compared to cation rings to get populated near the interface is also seen from the number density profile (Figure 3.15).

3.4 Conclusions

A force field model based on GAFF was refined – first, by adopting Maginn's force field parameters for the ether linkage and then refining the RESP charges to best represent several configurations through an iterative method. These refined parameters were then used to simulate the bulk liquid and the IL-vacuum interface. Due to the sluggish behaviour of OILs, multiple independent trajectories generated by a charge scaling procedure were used to analyze the results. Density and surface tension values from simulations are found to be in good agreement with experimental values. We've also found strong evidence for intramolecular hydrogen bonding between the ring hydrogens and the oxygen atoms of the linker. This intramolecular hydrogen bonding hinders the ring hydrogens from participating in intermolecular hydrogen bonding with anion atoms.

Bibliography

[1] Rogers, R. D.; Seddon, K. R.; Volkov, S. *Green Industrial Applications of Ionic Liquids*; Springer, 2002.

[2] Anderson, J. L.; Ding, R.; Ellern, A.; Armstrong, D. W. *J. Am. Chem. Soc.* **2005**, *127*, 593–604.

[3] Payagala, T.; Huang, J.; Breitbach, Z. S.; Sharma, P. S.; Armstrong, D. W. *Chemistry of Materials* **2007**, *19*, 5848–5850.

[4] Jin, C.-M.; Ye, C.; Phillips, B. S.; Zabinski, J. S.; Liu, X.; Liu, W.; Shreeve, J. M. *J. Mater. Chem.* **2006**, *16*, 1529–1535.

[5] Huang, K.; Han, X.; Zhang, X.; Armstrong, D. W. *Anal. and Bioanal. Chem.* **2007**, *389*, 2265–2275.

[6] Fang, D.; Yang, J.; Jiao, C. *ACS Catal.* **2011**, *1*, 42–47.

[7] Li, J.; Kang, Y.; Li, B.; Wang, X.; Li, D. *Energy & Fuels* **2018**, *32*, 12703–12710.

[8] Chen, Z. J.; Xue, T.; Lee, J.-M. *RSC Adv.* **2012**, *2*, 10564–10574.

[9] Huang, H.-C.; Yen, Y.-C.; Chang, J.-C.; Su, C.-W.; Chang, P.-Y.; Sun, I.-W.; Hsieh, C.-T.; Lee, Y.-L.; Teng, H. *J. Mater. Chem. A* **2016**, *4*, 19160–19169.

[10] Matsumoto, M.; Saito, Y.; Park, C.; Fukushima, T.; Aida, T. *Nat. Chem.* **2015**, *7*, 194–.

[11] Lian, C.; Su, H.; Liu, H.; Wu, J. *J. Phys. Chem. C* **2018**, *122*, 14402–14407.

[12] Matsumoto, M.; Shimizu, S.; Sotoike, R.; Watanabe, M.; Iwasa, Y.; Itoh, Y.; Aida, T. *J. Am. Chem. Soc.* **2017**, *139*, 16072–16075.

[13] Liu, Z.; Huang, S.; Wang, W. *J. Phys. Chem. B* **2004**, *108*, 12978–12989.

[14] Lopes, C. J. N.; Deschamps, J.; Pádua, A. A. *J. Phys. Chem. B* **2004**, *108*, 2038–2047.

[15] Lopes, C. J. N.; Deschamps, J.; Pádua, A. A. *J. Phys. Chem. B* **2004**, *108*, 11250–11250.

[16] Lopes, C. J. N.; Pádua, A. A. *J. Phys. Chem. B* **2004**, *108*, 16893–16898.

[17] Lopes, C. J. N.; Pádua, A. A. *J. Phys. Chem. B* **2006**, *110*, 19586–19592.

[18] Lopes, C. J. N.; Pádua, A. A.; Shimizu, K. *J. Phys. Chem. B* **2008**, *112*, 5039–5046.

[19] Mondal, A.; Balasubramanian, S. *J. Phys. Chem. B* **2014**, *118*, 3409–3422.

[20] Mondal, A.; Balasubramanian, S. *J. Phys. Chem. B* **2015**, *119*, 11041–11051.

[21] Florian, D.; Christian, H. *Phys. Chem. Chem. Phys.* **2013**, *15*, 2037–2049.

[22] Wang, J.; Wolf, R. M.; Caldwell, J. W.; Kollman, P. A.; Case, D. A. *J. Comput. Chem.* **2004**, *25*, 1157–1174.

[23] Jorgensen, W. L.; Maxwell, D. S.; Tirado-Rives, J. *J. Am. Chem. Soc.* **1996**, *118*, 11225–11236.

[24] Sambasivarao, S. V.; Acevedo, O. *J. Chem. Theory Comput.* **2009**, *5*, 1038–1050.

[25] Sprenger, K. G.; Jaeger, V. W.; Pfaendtner, J. *J. Phys. Chem. B* **2015**, *119*, 5882–5895.

[26] Barbosa, N. S. V.; Zhang, Y.; Lima, E. R. A.; Tavares, F. W.; Maginn, E. J. *J. Mol. Model.* **2017**, *23*, 194–207.

[27] Cieplak, P.; Cornell, W. D.; Bayly, C. I.; Kollman, P. A. *J. Comput. Chem.* **1995**, *16*, 1357–1377.

[28] Bayly, C. I.; Cieplak, P.; Cornell, W. D.; Kollman, P. A. *J. Phys. Chem.* **1993**, *97*, 10269–10280.

[29] Manz, T. A.; Sholl, D. S. *J. Chem. Theory Comput.* **2012**, *8*, 2844–2867.

[30] Manz, T. A.; Sholl, D. S. *J. Chem. Theory Comput.* **2010**, *6*, 2455–2468.

[31] Wendler, K.; Dommert, F.; Zhao, Y. Y.; Berger, R.; Holm, C.; Site, L. D. *Faraday Discuss.* **2012**, *154*, 111–132.

[32] Dennington, R.; Keith, T.; Millam, J. GaussView Version 5. Semichem Inc., Shawnee Mission, KS, 2009.

[33] Frisch, M. J. et al. Gaussian 09 Revision D.01. Gaussian Inc. Wallingford CT **2009**.

[34] Dupradeau, F.-Y.; Pigache, A.; Zaffran, T.; Savineau, C.; Lelong, R.; Grivel, N.; Lelong, D.; Rosanski, W.; Cieplak, P. *Phys. Chem. Chem. Phys.* **2010**, *12*, 7821–7839.

[35] Nosé, S. *J. Chem. Phys.* **1984**, *81*, 511–519.

[36] Nosé, S. *Mol. Phys.* **1984**, *52*, 255–268.

[37] Martyna, G. J.; Klein, M. L.; Tuckerman, M. *J. Chem. Phys.* **1992**, *97*, 2635–2643.

[38] Ryckaert, J.-P.; Ciccotti, G.; Berendsen, H. J. C. *J. Comput. Phys.* **1977**, *23*, 327–341.

[39] Plimpton, S. *J. Comput. Phys.* **1995**, *117*, 1–19.

[40] Brown, W. M.; Peng, W.; Plimpton, S. J.; Tharrington, A. N. *Comput. Phys. Commun.* **2011**, *182*, 898–911.

[41] Brown, W. M.; Kohlmeyer, A.; Plimpton, S. J.; Tharrington, A. N. *Comput. Phys. Commun.* **2012**, *183*, 449–459.

[42] Martinez, L.; Andrade, R.; Birgin, E. G.; Martinez, J. M. *J. Comput. Chem.* **2009**, *30*, 2157–2164.

[43] Salanne, M.; Simon, C.; Turq, P. *The Journal of Physical Chemistry B* **2006**, *110*, 3504–3510.

[44] Bhargava, B. L.; Balasubramanian, S. *J. Phys. Chem. B* **2008**, *112*, 7566–7573.

[45] Moosavi, M.; Khashei, F.; Sedghamiz, E. *Phys. Chem. Chem. Phys.* **2018**, *20*, 435–448.

[46] Freire, M. G.; Carvalho, P. J.; Fernandes, A. M.; Marrucho, I. M.; Queimada, A. J.; Coutinho, J. A. *J. Colloid Interf. Sci.* **2007**, *314*, 621 – 630.

[47] Bhargava, B. L.; Balasubramanian, S. *J. Am. Chem. Soc.* **2006**, *128*, 10073–10078.

Chapter 4

Summary and Future Outlook

The thesis explicates the work on three major aspects of modelling ionic liquids: (i) understanding the charge environment in imidazolium based binary ionic liquid mixtures and incorporating the charges into a force field framework, (ii) investigating the hydrogen bond dynamics in binary ionic liquid mixtures and (iii) development and validation of a force field for oligomeric ionic liquids (OILs).

Chapter 2A describes the investigation of the charge environment in an imidazolium-based binary ionic liquid mixture, [BMIM][Cl][BF_4]. Analysis of the net ion charges estimated from condensed phase periodic DFT calculations showed that the cation's (BMIM) charge varies linearly with anion composition, whereas the anion charges remain invariant. Our result segues well with the experimental findings of Licence *et al.*

In the present study we concentrate on binary ionic liquid mixtures containing a single cation and two different anions. This framework to study charge environment could be extended to study binary ionic liquid mixtures containing single anion and two different anions. Teng *et al.* used a binary ionic liquid mixture containing a common anion and two different cations (monomeric and dicationic) to optimized EDL capacitance of the mixture (see chapter 2B.4. Hence understanding charge environment of such binary mixtures can help improve MD simulations of such mixtures as well.

A systematic comparison of static and dynamic properties of other binary ionic liquid

mixtures, predicted by MB force field using linear mixture rule, can further improve the confidence in the force field. Further, interfacial structure of binary ionic liquids could be studied to investigate selective enrichment near the surface.

Chapter 2B describes the hydrogen bond exchange process in the same binary mixture.The hydrogen bond switching is shown to be a three step process involving hydrogen bond breaking, relative diffusion and hydrogen bond forming respectively. The timescales of each of these processes have been determined which rationalize the differences in experimental results of IR and NMR spectroscopies.

Chapter 3 describes the validation of a force field for a new class of ionic liquids called oligomeric ionic liquids (OILs). Density and surface tension values from simulations are found to be in good agreement with experimental values. We have also found strong evidence for intramolecular hydrogen bonding between the ring hydrogens and the oxygen atoms of the linker. This intramolecular hydrogen bonding hinders the ring hydrogens from participating in intermolecular hydrogen bonding with anion atoms. The refinement procedure developed in this work could be applied to refine the force field parameters of higher oligomers of the cation (IL3, IL4). A comparative study of monomeric and oligomeric ionic liquids can yield crucial microscopic insights into the structure and dynamics of the electric double layers formed by these systems. Further, mesoscopic structure could be studied to examine any structural differences between monomeric and oligomeric ionic liquids.

Appendix

Table 4.1: Optimized RESP charges used to simulate [IL2][NTf_2] system.

Atom	Charge	Atom	Charge	Atom	Charge	Atom	Charge	Atom	Charge
C1	-0.2401	H20	0.0140	C39	-0.0078	H58	0.0015	F77	-0.1042
H2	0.2407	H21	0.0140	H40	0.1001	C59	-0.0355	C78	0.3362
C3	-0.1137	C22	-0.0078	H41	0.1001	H60	0.0140	S79	0.6368
H4	0.1993	H23	0.1001	N42	0.0027	H61	0.0140	N80	-0.4699
N5	0.0307	H24	0.1001	C43	0.1035	H62	0.0140	S81	0.6368
N6	0.0027	C25	0.0433	H44	0.1679	C63	0.3362	C82	0.3362
C7	0.1035	H26	0.0606	C45	-0.1137	S64	0.6368	O83	-0.4283
H8	0.1679	H27	0.0606	H46	0.1993	N65	-0.4699	O84	-0.4283
C9	-0.0465	O28	-0.3248	C47	-0.2401	S66	0.6368	O85	-0.4283
H10	0.1191	C29	0.0789	H48	0.2407	C67	0.3362	O86	-0.4283
H11	0.1191	H30	0.0547	N49	0.0307	O68	-0.4283	F87	-0.1042
C12	-0.0175	H31	0.0547	C50	-0.0465	O69	-0.4283	F88	-0.1042
H13	0.0180	C32	0.0789	H51	0.1191	O70	-0.4283	F89	-0.1042
H14	0.0180	H33	0.0547	H52	0.1191	O71	-0.4283	F90	-0.1042
C15	0.0312	H34	0.0547	C53	-0.0175	F72	-0.1042	F91	-0.1042
H16	0.0015	O35	-0.3248	H54	0.0180	F73	-0.1042	F92	-0.1042
H17	0.0015	C36	0.0433	H55	0.0180	F74	-0.1042		
C18	-0.0355	H37	0.0606	C56	0.0312	F75	-0.1042		
H19	0.0140	H38	0.0606	H57	0.0015	F76	-0.1042		

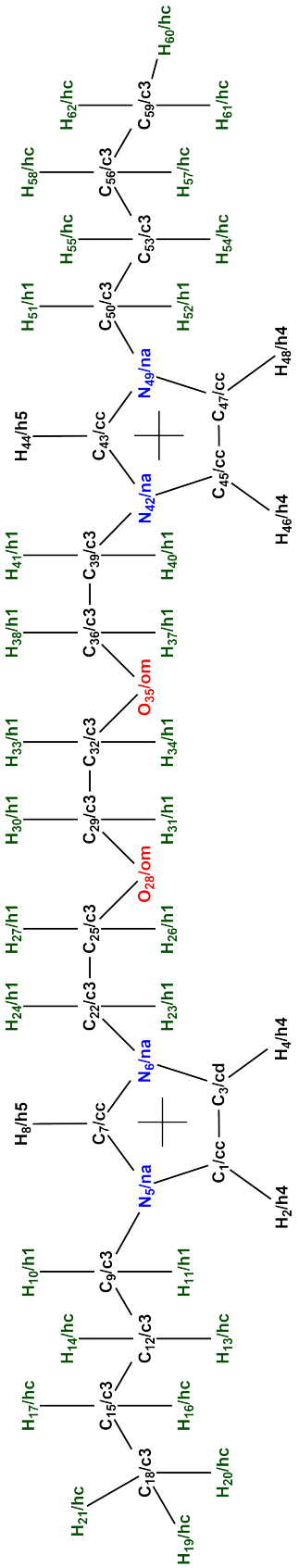

Figure 4.1: Chemical structure of IL2 cation along with atom name and atom type used in this study (atom name/atom type).